

Polarization selectivity in fifth-order electronically nonresonant Raman scattering from CS₂

Laura J. Kaufman, David A. Blank,^{a)} and Graham R. Fleming
*Department of Chemistry, University of California, and Physical Biosciences Division,
Ernest Orlando Lawrence Berkeley National Laboratory, Berkeley, California 94720*

(Received 22 August 2000; accepted 8 November 2000)

This paper presents several experimentally collected tensor elements of the direct fifth-order Raman signal of room temperature CS₂. All results were collected so as to reduce contamination from third-order cascade signals, and it is shown that while these cascade signals are of varying importance in different tensor elements, phase matching considerations are sufficient to make the direct fifth-order signal the dominant signal in every tensor element collected. We show, as predicted, that the different tensor elements appear to weight particular Liouville pathways of the direct fifth-order signal, and thus particular dynamics of the studied system, differently. The magic angle signals are shown to contain information about the intermolecular vibrational echo and to put a limit on the time scale of rephasing of the room temperature liquid. The R_{yzzzy} tensor element, in conjunction with the R_{yyzzz} tensor element, is shown to be useful in studying the pure dephasing and population dynamics of the liquid. From these data it appears that population dynamics occur on a much longer time scale than pure dephasing dynamics, even though this is not obvious for the intermolecular motions of a room temperature liquid that are studied here. Further, intensities and behaviors of different tensor elements of the experimental data are compared with the only detailed theory currently available that explicitly includes polarization dependence. © 2001 American Institute of Physics. [DOI: 10.1063/1.1337042]

I. INTRODUCTION

Much experimental and theoretical attention has been given to the development of time-domain nonresonant fifth-order Raman spectroscopy since Tanimura and Mukamel proposed it as a means to separate homogeneous and inhomogeneous contributions to vibrational line shapes.¹ It was later pointed out that the technique could not only separate homogeneous and inhomogeneous contributions to line shapes, but also was potentially a sensitive probe of couplings between nuclear motions: this stimulated further efforts to develop the experimental technique and the theoretical basis of this powerful, new spectroscopy.²⁻²⁹

The potential of this technique to both deconvolute contributions to line shapes and probe couplings between modes rests in the fact that the fifth-order nonresonant Raman experiment gives no signal unless a nonlinearity in the polarizability and/or the mechanical potential is probed. The experiment begins with an electronically nonresonant Raman excitation of a system by two ultrafast laser pulses, leaving the system in a superposition state of two vibrational levels, a vibrational coherence. After a time delay, a second pair of ultrafast pulses can transfer the system to a second superposition state or to a population state. After a second time delay, a final pulse stimulates a Raman scattering event in a particular phase matched direction. The fact that the two states induced by the first two sets of pulses may be superposition states that have nearly equal and opposite time-

evolution (as determined by the frequency differences between the vibrational levels involved in the two states) allows for rephasing.¹ Rephasing effects removal of inhomogeneous contributions to the line shapes for certain values of the two time-delays involved. Generation of these echo-type responses, as well as all generated fifth-order Raman signals, requires either that one of the transitions initiated by the sets of pulses is a two or zero quantum transition or that a one quantum transition induced by a pulse pair effectively becomes a zero or two quantum transition during the second variable time period.^{19,30} Such transitions can occur only if a nonlinearity in the polarizability and/or a vibrational anharmonicity is present:^{1,2,19,23,30} thus the fifth-order signal has the potential to be an exquisitely sensitive probe of both the nature and magnitude of coupling between nuclear motions of a system. While such information content allows this experiment to be viewed as an optical analogue to 2D-NMR with vastly increased time-resolution, the dependence of the signal on these nonlinearities ensures that the signal magnitude will be significantly reduced compared to signals with no such dependence.²⁹

It has been shown that previous attempts to measure the fifth-order signal had, in fact, measured third-order cascade signals, which contain no more information than ordinary third-order electronically nonresonant measurements.²⁵ Such signals do not depend on the nonlinearities discussed above and unless carefully avoided will dominate the desired direct fifth-order response. It has recently been shown that by careful consideration of the phase matching requirements for the cascade and the direct fifth-order signals, serious contamina-

^{a)}Present address: Department of Chemistry, University of Minnesota, Minneapolis, MN 55455-0431.

tion of the direct fifth-order signal by cascades can be avoided.²⁹ Other efforts are currently underway to use inherently phase-sensitive heterodyne detection to separate contributions from the cascade and direct fifth-order signals based on the difference between the phases of the signals.^{24,27,28} In this manuscript we report on direct fifth-order signals collected with homodyne detection with an incoming beam geometry carefully chosen to greatly reduce contamination due to third-order cascade signals. Several tensor elements of the signal have been collected, and we report observations on polarization selectivity that show qualitative agreement with theoretical studies to date. These observations relate to the relative magnitudes of the tensor elements of the direct fifth-order signals and to the apparent selective weighting different tensor elements give to different Liouville pathways such as the rephasing pathway mentioned above.

II. EXPERIMENT

A. Experimental setup

As discussed in detail elsewhere, a standard titanium sapphire oscillator was used to generate 1 nJ, 28 fs [Gaussian, full width at half maximum (FWHM)] pulses centered at 800 nm.³¹ The pulses were regeneratively amplified resulting in 25 μJ/pulse, 48 fs, 800 nm pulses at a repetition rate of 1.5 kHz.³² Pulse duration was determined by off-axis autocorrelations in a 150 μm BBO crystal. The regenerative amplifier was pumped by a Q-switched, diode-pumped Nd:YLF (LightWave Electronics) with shot-to-shot root-mean-squared intensity fluctuations of <0.5% at 532 nm resulting in very small power fluctuations at the sample. Following attenuation to approximately 10 μJ/pulse, the pulse was split into five pulses of nearly equal intensity, ~2 μJ per pulse per beam. Mechanical translation stages with stepping resolution of 0.1 μm (Newport) were used to sweep the two adjustable time variables, τ₂ and τ₄, in such a way as to collect surfaces as a function of the two time delays between the pairs of laser pulses directly.²⁵ The polarization of each beam was individually adjusted by a λ/2 waveplate. The five beams were focused into a 1.0 mm sample cell containing CS₂ at room temperature with a 28.9 cm focal length singlet lens. The fifth-order signal emerged in a phase matched direction described in detail below. Irises were used to spatially select the signal, which was filtered through an 800±20 nm filter and detected using an IR extended photo-multiplier tube (Hamamatusa, R636-10). To assist in spatial location of the signal, a sixth beam aligned along the signal direction was used to arrange the detection setup and was blocked before data collection began. One of the five incoming beams was mechanically chopped at half the laser repetition rate, and the signal was collected by a lock-in amplifier synchronized to the mechanical chopping frequency.

B. Phase matching

We have previously shown that early measurements of fifth-order electronically nonresonant Raman responses from the intermolecular motions of CS₂ were dominated by third-order cascade signals, which emerge in an experimentally inseparable phase matched direction from the direct fifth-

order signal.²⁵ It was shown that the two-step nature of the cascade signals could be exploited to greatly diminish the magnitude of the cascade responses in the measured fifth-order signal.^{25,29} This was accomplished by poorly phase matching the first step of each of the four cascade processes while leaving the overall fifth-order process well phase matched. The phase matching geometry with which we accomplished this is depicted in Fig. 1(a). In this paper, we will give a more quantitative picture of the phase matching considerations in an effort to assess the ratio of cascade to direct fifth-order responses in our geometry chosen expressly to suppress cascade contributions.

The signal is measured along the phase matched direction $k_{s5} = (k_1 - k_2) - (k_3 - k_4) + k_5$. Both the cascade and direct fifth-order signals emerge in this direction. The two types of cascade responses are the symmetric cascades, which are symmetric in the two adjustable time variables (τ₂ and τ₄), and the parallel cascades, which are symmetric in τ₄ and τ₂ + τ₄.^{24–26,33} Figures 1(b) and 1(c) schematically show the excitation and emission events for the direct fifth-order process and for the cascade processes. The symmetric cascades have two possible intermediate steps, k_{s1} and k_{s2} , which emerge with the wave vectors $k_{s1} = k_1 - k_2 - k_3$ and $k_{s2} = k_1 - k_2 + k_4$. The parallel cascades have two possible intermediate steps, k_{p1} and k_{p2} , which emerge with the wave vectors $k_{p1} = k_1 - k_2 + k_5$ and $k_{p2} = -k_3 + k_4 + k_5$. Each cascade uses an emitted field produced by a third-order scattering event to either pump (symmetric cascades) or probe (parallel cascades) another third-order scattering event on a separate chromophore. The time dependent responses for the two types of cascades in terms of the third-order response functions are shown in Eqs. 1(a) and 1(b):

$$R_{nmlkji, \text{sequential}}^{(3)^2} = R_{\text{seq}}^{(5)}(\tau_2, \tau_4) \\ = R_{\sigma k ji}^{(3)}(\tau_2) R_{nml\sigma}^{(3)}(\tau_4) \\ + R_{\sigma l ji}^{(3)}(\tau_2) R_{nmk\sigma}^{(3)}(\tau_4), \quad (1a)$$

$$R_{nmlkji, \text{parallel}}^{(3)^2} = R_{\text{par}}^{(5)}(\tau_2, \tau_4) \\ = R_{\sigma m ji}^{(3)}(\tau_2 + \tau_4) R_{n\sigma lk}^{(3)}(\tau_4) \\ + R_{\sigma mlk}^{(3)}(\tau_4) R_{n\sigma ji}^{(3)}(\tau_2 + \tau_4). \quad (1b)$$

The subscripts, *i-n*, refer to the relative polarizations of the incoming laser fields and of the signal field. By convention the time-ordering of the subscripts reads from right to left with the right-most label referring to the first pulse and the left-most label describing the signal field polarization.

Typically, a phase matching factor is expressed as a number from 0 to 1 (with 1 being perfect phase matching) described by the expression sinc(Δ*k*l/2) with 1 the length of the sample cell and Δ*k* the phase mismatch.³⁴ This expression depends on the assumption that there is no variation in the product of the amplitudes of the incoming beams as a function of distance along the sample, *z*.²⁹ While our incoming beams approach the sample at small angles from the normal of the sample face, there is still a significant *z* dependence of the amplitude product of the incoming beams within our 1 mm sample path length. In a recent paper we

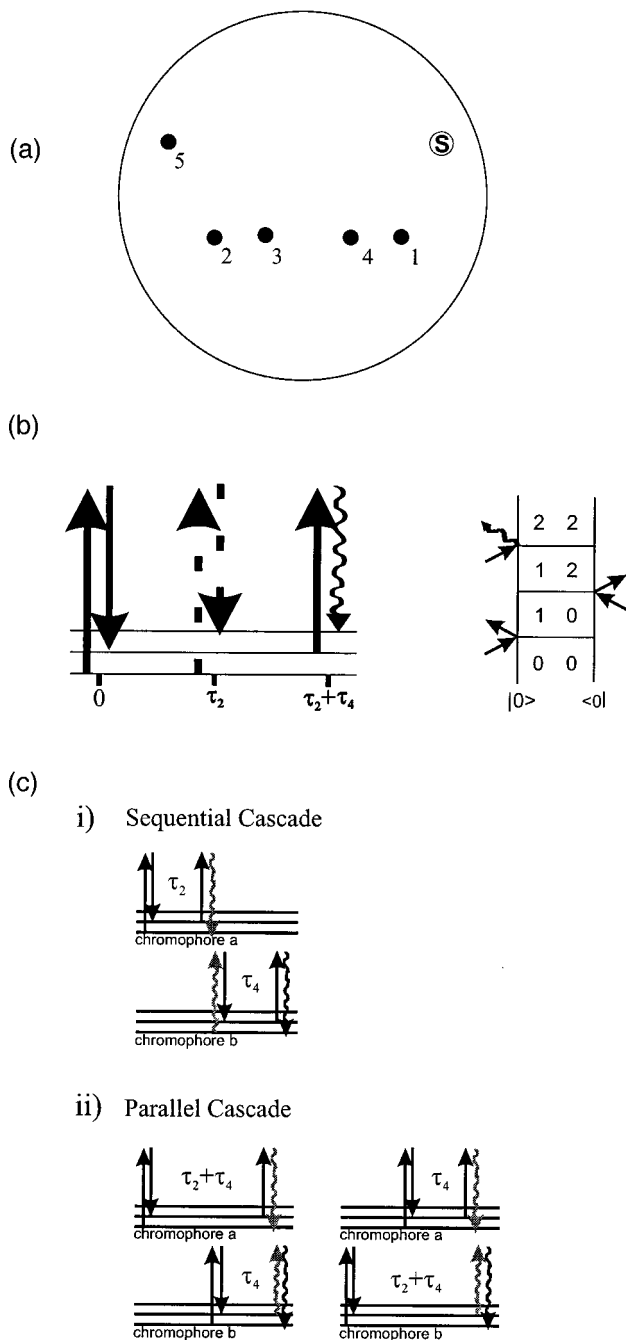


FIG. 1. (a) The phase matching geometry used in this experiment: the numbered circles are the incoming fields, and the circle labeled "S" is the signal field in the x - y plane orthogonal to the axis of propagation, z . (b) Ladder diagram and Feynman diagram showing one of the Liouville pathways of the fifth-order Raman experiment. In the ladder diagram solid lines represent a ket side interaction and dashed lines indicate a bra side interaction. In the Feynman diagram time runs up and the numbers indicate the vibrational state of the excited oscillator. In both diagrams the wavy line represents the emitted field. (c) Ladder diagrams for (i) one of the two sequential cascades and (ii) both of the parallel cascades.

accounted for this by analytically solving an integral that accounts for the z -dependence of the spatial overlap between the incoming beams.²⁹ The value of this integral was termed the phase matching factor, and it was calculated for the direct fifth-order process and for the first step in each of the four cascades. Minimization procedures allowed determination of the beam geometry used both in Ref. 29 and in the experi-

ments discussed here [Fig. 1(a)]. Such calculations, however, do not account for the second step in the cascade and thus the overall degree of phase matching for the cascade processes. To correctly account for the complete cascade processes, the signal field generated from the first step of the cascade, which develops at some angle to the normal of the sample face and with some z -dependent amplitude build-up through the sample, must be considered. Here we account for this generated field that participates in the second step of the cascade. This will allow for a more quantitative accounting of the cascade and cascade/direct fifth-order cross-terms in the signals collected in the geometry used here and in Ref. 29 to be made. As in the previous calculations, it is assumed that the incoming laser pulses have Gaussian transverse amplitude profiles. In this calculation this form is also assumed for the generated signal beam that emerges from the first step of the cascade processes.

We start from the Maxwell equation for the amplitude of the signal field using the n -order induced polarization as the source term,

$$\begin{aligned} \nabla \times \nabla \times \{ \epsilon_s^{(n)}(r, t) \exp(ik'_s \cdot r) \} - \frac{n_s^2 \omega_s^2}{c^2} \epsilon_s^{(n)}(r, t) \exp(ik'_s \cdot r) \\ = \frac{4\pi\omega_s^2}{c^2} \bar{P}_s^{(n)}(t) \exp(ik_s \cdot r). \end{aligned} \quad (2)$$

Here, k_s is the combination of incoming wave vectors and k'_s is the wave vector of the generated field. A solution is found of the form

$$\epsilon_s^{(n)}(t) = \frac{\omega_s^2}{|k'_s|^2 c^2} \int dz P_s^{(n)}(t, z) \exp(i\Delta k \cdot z) \quad (3)$$

using the assumption that the signal field is emitted along the z direction. In this equation $\Delta k = k_s - k'_s$. The difference of a factor of $2\pi i$ in Eq. (3) as compared to Eq. (3) in Ref. 29 is accounted for within the integral in the expression presented here. It was previously taken out of the integral through analogy with the expression for the electric field given when phase matching is considered within the $\text{sinc}(\Delta k l/2)$ approximation. However, in the formulation to be used here, the $2\pi i$ factor is not brought outside the integral in a straightforward manner and is therefore left inside the integral in all expressions that follow. The n -order induced polarization can be expressed in terms of the n -order response function, $R^{(n)}$,

$$P^{(n)}(t_1, \dots, t_{(n/2-1)}, z) = NO^{(n)}(z)R^{(n)}(t_1, \dots, t_{(n/2-1)}), \quad (4)$$

where $O^{(n)}(z)$ is the z -dependent amplitude product of the n incoming fields, $\epsilon_1(z)\epsilon_2(z)\dots\epsilon_n(z)$, and N is the number density of chromophores.

For the generated direct fifth-order field, expressing $O^{(5)}(z)$ as the normalized spatially z -dependent overlap of the five incoming beams, $o^{(5,4,3,2,1)}(z)$, multiplied by the magnitude of the product of the five incoming beams when perfectly overlapped, $O^{(5)}$, the signal field amplitude is

$$\epsilon_s^{(5)}(\tau_2, \tau_4) = \frac{\omega_s^2}{|k'_s|c^2} NO^{(5)}R^{(5)}(\tau_2, \tau_4) \times \int_0^l dz o^{(5,4,3,2,1)}(z) \exp(i\Delta k \cdot z). \quad (5)$$

The integral over z can be used to compare relative degrees of phase matching between different geometries of incoming beams, and we define this as the phase matching factor, $F^{(5)}$. Similarly, the first step in a cascade process generates a signal field given by

$$\epsilon_s^{(3)}(\tau_2) = \frac{\omega_s^2}{|k'_s|c^2} NO^{(3)}R^{(3)}(\tau_2) \int_0^l dz o^{(3,2,1)}(z) \exp(i\Delta k \cdot z). \quad (6)$$

To correctly account for the phase matching of the second step in the cascade, the buildup of the generated signal $\epsilon_s^{(3)}$ through the sample must be accounted for. Then, the overall generated cascade field can be expressed as follows:

$$\epsilon_s(\tau_2, \tau_4) = \frac{\omega_s^2}{|k'_s|c^2} \frac{\omega_{si}^2}{|k'_{si}|c^2} N^2 O^{(2)} O^{(3)} R^{(3)}(\tau_2) R^{(3)}(\tau_4) \times \int_0^l dz o^{(5,4)}(z) \exp(i\Delta k \cdot z) \times \int_0^z dz' o^{(3,2,1)}(z') \exp(i\Delta k' \cdot z'). \quad (7)$$

Here, the ω_{si} and k'_{si} factors refer to the frequency and wave vector of the intermediate signal emitted in the cascade. This equation is inexact in that to truly account for the amplitude build-up of the intermediate field through the sample along z , we must look for a solution of a different form for the Maxwell equation, and this solution for the generated field should be used for the intermediate cascade field.

While the double integral in Eq. (7) gives a phase matching factor for the overall cascade process, this number is not directly comparable to the phase matching number for the direct fifth-order process. The two integrals differ by a factor of length, which is recovered in the extra $\omega_s^2/(|k'_s|c^2)$ factor present in the cascade expression. Even with this inclusion, which makes the units of the phase matching numbers the same for the cascade and direct fifth-order signals, the two numbers are difficult to compare since they do not include the different orders of N , $R^{(3)}$, and $R^{(5)}$ factors present in the two signals. Despite this difficulty comparing phase matching numbers for different terms, comparing phase matching numbers for the four cascade processes to each other for a given geometry of incoming beams is straightforward, as is comparing phase matching ratios between each of the cascade and direct fifth-order signals between geometries.

III. RESULTS

Several tensor elements were collected in the geometry used in Ref. 29 and are presented here. The R_{zzzzzz} signal is shown, as are several other tensors: R_{yyzzzz} , R_{zyzyzz} , R_{yzzyzy} , R_{zzzzmm} , R_{zzmmzz} , and R_{mmzzzz} (Figs. 2 and 3). As discussed previously, the measured signal intensity is fifth-order in the total incoming intensity of the five beams.²⁹ The

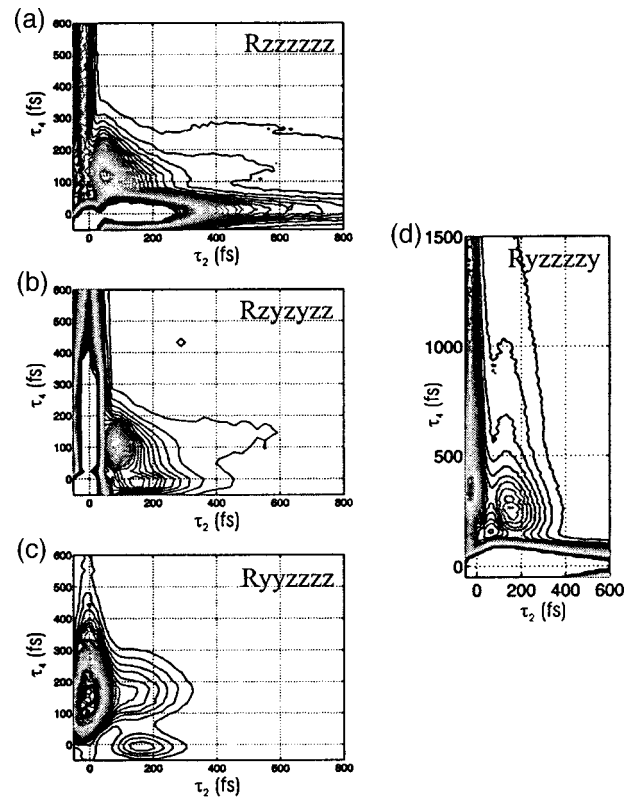


FIG. 2. Contour plots of two-dimensional fifth-order signals of room temperature CS₂ collected using the phase matching geometry in Fig. 1(a) and of Ref. 29). Different tensor elements are shown: (a) R_{zzzzzz} , (b) R_{zyzyzz} , (c) R_{yyzzzz} , and (d) R_{yzzyzy} .

measured signals vary greatly in intensity, and a plot of slices at $\tau_4 = 180$ fs displaying these intensity differences is shown later. These signals are all homodyne detected and therefore measure the intensity of the direct fifth-order response. The measured R_{zzzzzz} signal [Fig. 2(a)] was previously discussed in Ref. 29. It peaks at $\tau_2 \sim 60$ fs and $\tau_4 \sim 110$ fs. It is rather symmetric about τ_2 and τ_4 . There is a small asymmetric component that extends along $\tau_2 \sim 120$ fs. The signal on the $\tau_4 = 0$ fs axis is stronger than that on the $\tau_2 = 0$ fs axis, although both extend beyond one picosecond. The R_{zyzyzz} signal [Fig. 2(b)] also peaks in the two-dimensional area ($\tau_2 > 0$ fs, $\tau_4 > 0$ fs), at $\tau_2 \sim 80$ fs, $\tau_4 \sim 100$ fs. This signal is also quite symmetric, with a very small extension along the τ_2 dimension, similar to that seen in the R_{zzzzzz} signal. On the axes, this signal is much more intense along $\tau_4 = 0$ fs than along $\tau_2 = 0$ fs. Similarly, the R_{yyzzzz} signal [Fig. 2(c)] has a longer, more intense signal along $\tau_4 = 0$ fs than along $\tau_2 = 0$ fs. The signal around the $\tau_2 = 0$ fs axis is intense and not pulse-width limited. The signal does not peak away from the $\tau_2 = 0$ fs axis, and it falls off very quickly and symmetrically about the τ_2 and τ_4 axes as compared to the R_{zzzzzz} signal. The R_{yzzyzy} signal [Fig. 2(d)] shows significantly different features than any of the tensor elements discussed previously. The signal in the two-dimensional area has a strikingly elongated feature along the τ_4 dimension with the peak of the signal at $\tau_2 \sim 160$ fs, $\tau_4 \sim 260$ fs. The signal extends to several picoseconds along the τ_4 dimension, as does the signal on the $\tau_2 = 0$ fs axis, which is much less intense than the signal on the $\tau_4 = 0$ fs axis.

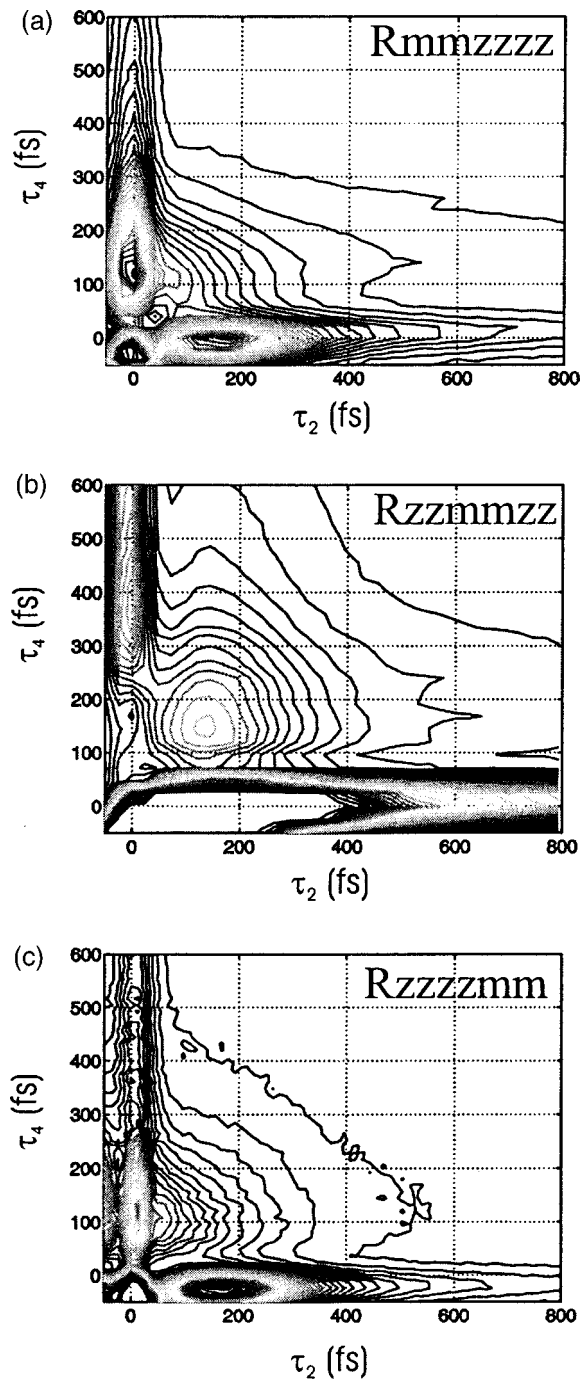


FIG. 3. Contour plots of the magic angle tensor elements of the two-dimensional fifth-order signal of room temperature CS_2 : (a) R_{mmzzzz} , (b) R_{zzmmzz} , and (c) R_{zzzzmm} .

The other three tensor elements presented are magic angle signals. In each of these, one pulse pair was set at an angle of 54.7° relative to the other pulse pairs. This is the angle regularly used in third-order spectroscopy to selectively probe isotropic dynamics.^{20,35–37} Such absolute selection for isotropic dynamics is not possible in fifth-order Raman spectroscopy,³⁸ but the magic-angle signals may still contain interesting and different information from that evident in the other tensor elements collected. The R_{zzzzmm} signal [Fig. 3(c)] peaks on the $\tau_2 = 0$ fs axis and decays within 500 fs along τ_2 and even more quickly along τ_4 . The signals

on the axes are of approximately equal intensity and decay on similar time scales. The R_{mmzzzz} signal [Fig. 3(a)] appears similar to the R_{zzzzmm} signal with the exception of a stronger $\tau_4 = 0$ fs signal and a concomitant extension of the signal out to approximately one picosecond along τ_2 . The R_{zzmmzz} signal [Fig. 3(b)], on the other hand, peaks at $\tau_2 \sim 180$ fs, $\tau_4 \sim 140$ fs. It extends along both time dimensions, with a somewhat greater extension along τ_4 . This signal falls off remarkably slowly compared to that of the R_{mmzzzz} and R_{zzzzmm} surfaces, and it begins to show some echolike behavior along the $\tau_2 = \tau_4$ ridge as will be discussed below. In this tensor element, like many of the others discussed, the signal along the $\tau_4 = 0$ fs axis is more intense and decays faster than the signal on the $\tau_2 = 0$ fs axis.

IV. DISCUSSION

A. Fifth-order response

The fifth-order response has been discussed in detail previously.^{1,3,10,12,18,19,23,30,39} The response consists of three hyperpolarizability responses, Eqs. 8(a)–8(c), and a three-point polarizability correlation function, Eq. 8(d). While each term is part of the direct fifth-order signal, term 8(d) will be the contribution discussed most frequently. It is the only term that can contribute to the measured signal away from both axes.

$$R_{nmkji}^{(5)}(\tau_2, \tau_4) \propto \langle \xi_{nmkji} \rangle \delta(\tau_2) \delta(\tau_2 + \tau_4) \quad (8a)$$

$$+ \frac{i}{4\hbar} \langle [\alpha_{nm}(\tau_4), \gamma_{lkji}(0)] \rangle \delta(\tau_2) \quad (8b)$$

$$+ \frac{i}{2\hbar} \langle [\gamma_{nmk}(\tau_2), \alpha_{ji}(0)] \rangle \delta(\tau_4) \quad (8c)$$

$$- \frac{1}{4\hbar^2} \langle [[\alpha_{nm}(\tau_2 + \tau_4), \alpha_{lk}(\tau_2)], \alpha_{ji}(0)] \rangle. \quad (8d)$$

Here, $\alpha_{nm}(t)$ is the polarizability response induced at time t by the nm -polarized pulse pair. Taylor expanding the polarizability operator in terms of coordinates q_a gives

$$\alpha(t) = \alpha_0 + \sum_a \alpha_a^{(1)} q_a(t) + \frac{1}{2} \sum_{a,b} \alpha_{ab}^{(2)} q_a(t) q_b(t) + \dots, \quad (9)$$

where $\alpha_a^{(n)}$ is the n -th derivative of the polarizability with respect to the coordinate of the a -th oscillator. Here the tensorial nature of these operators is suppressed for clarity. Assuming harmonic potentials and truncation of the Taylor expansion at first order in q (Placzek approximation), the three-point polarizability correlation function that appears in Eq. 8(d) will be exactly zero. This three-point polarizability correlation function is responsible for all fifth-order signal away from the time axes. Thus the generation of fifth-order signal away from the time axes requires the presence of anharmonicity in the potential and/or nonlinearity in the polarizability.^{1,4,12,39} Then, the portion of the direct fifth-order signal that arises from term 8(d) can be expressed as

$$R^{(5)}(\tau_2, \tau_4) = R^{(5),AN}(\tau_2, \tau_4) + R^{(5),NP}(\tau_2, \tau_4), \quad (10)$$

with AN referring to the signal arising from anharmonicity in the potential and NP referring to that arising from nonlinearity in the polarizability. Either of the two nonlinearities al-

lows for a two or zero quantum transition, a transition present in all Liouville pathways that allow for fifth-order signal generation. For the signal generated through nonlinear polarizability, this two or zero quantum transition must occur coincident with the interaction of a pulse pair and the sample. For the signal generated through anharmonicity, this two or zero quantum transition is effected later: a one quantum interaction occurs coincident with the first and second pulse pairs and an anharmonic interaction between modes makes this effectively a two or zero quantum transition during the second variable time period. In signal arising from anharmonicity, the three-point polarizability correlation function can be expressed as products of two-point correlation functions regularly used to express third-order response functions.^{1,3,39} The signal is then expressed as

$$R^{(5),\text{AN}}(\tau_2, \tau_4) \propto \sum_{a,b,c} g_{abc}^{(3)} \alpha_a^{(1)} \alpha_b^{(1)} \alpha_c^{(1)} \times \int_0^\infty d\tau \langle [q_a(\tau_4), q_a(\tau)] \rangle \langle [q_b(\tau), q_b(0)] \rangle \times \langle [q_c(\tau_2), q_c(\tau)] \rangle \quad (11)$$

with $g_{abc}^{(3)}$ the magnitude of the cubic anharmonicity also typically expressed as $V^{(3)}(q)$, the third derivative of the potential with respect to the coordinate. As in Eq. (9), beam polarizations have been suppressed in this expression. This expression is obtained through the use of Wick's theorem and a perturbative treatment of the anharmonicity. It has been shown recently that if the factorization using Wick's theorem is not applied, a different expression for the anharmonic term, which reflects the non-Markovian fluctuations of the system-bath interaction and level dependent vibrational dephasing, results.⁴⁰

Similarly the nonlinear polarizability contribution to the signal can be expressed as

$$R^{(5),\text{NP}}(\tau_2, \tau_4) \propto \sum_{a,b} [\alpha_{ab}^{(2)} \alpha_a^{(1)} \alpha_b^{(1)} \langle [q_a(\tau_4), q_a(0)] \rangle \times \langle [q_b(\tau_2 + \tau_4), q_b(0)] \rangle + \alpha_a^{(1)} \alpha_{ab}^{(2)} \alpha_b^{(1)} \times \langle [q_a(\tau_4), q_a(\tau)] \rangle \langle [q_b(\tau_2), q_b(0)] \rangle], \quad (12)$$

where $\alpha_{ab}^{(2)}$ is the second derivative of the polarizability with respect to the coordinate for modes a and b , and, for cases where $a \neq b$, expresses the coupling between modes a and b induced by the interaction with light.^{1,3,39} Again, it has recently been shown that a third term should be present in this expression even in the case of Markovian system-bath interactions. This term arises from level-dependent vibrational dephasing and describes a Liouville pathway in which the $\alpha^{(2)}$ interaction occurs with the first set of pulses.^{17,40} In the approximated $R^{(5),\text{NP}}(\tau_2, \tau_4)$ of Eq. (10), the $\alpha^{(2)}$ interaction necessarily occurs in the second or third step of the experiment. Within the approximated response functions presented in Eqs. (11) and (12), the terms $g_{abc}^{(3)}$ and $\alpha_{ab}^{(2)}$ hold the potential information on the magnitude of coupling between nuclear motions that this experiment can probe.

However, it is also the presence of these terms that prevents the modeling of the fifth-order response of intermo-

lecular modes of a system with the third-order response. The reasons the third-order response is an inappropriate basis for the fifth-order response of intermolecular modes have been discussed in detail elsewhere.^{20,22,29} So, to gain insight into the meaning of the measured fifth-order response and dynamics of the system, comparisons to instantaneous normal mode (INM) analysis, quenched normal mode (QNM) analysis, and molecular dynamics (MD) simulations will play a key role.

B. Measured signals

As discussed in Ref. 29, despite good agreement with the QNM analysis presented in Ref. 18, it was noted that our R_{zzzzzz} data and the simulations differed in that the data displayed a small extension along τ_2 , a feature not seen in the simulations. Because QNM simulations cannot capture diffusive dynamics, it is possible that the difference between data and simulation is due to the presence of these dynamics (or a cross-term between these and other dynamics) in the measured direct fifth-order signal. However, in part because simulations show that lower frequency motions may show up less strongly in the direct fifth-order signal than in the third-order signal,^{21,22} this extension of the signal was previously suggested to be due to, not diffusive dynamics, but a residual cascade signal or a cross-term between a cascade signal and the direct fifth-order signal.²⁹ Here, our more complete accounting of the phase matching factors allows us to discuss this in greater detail.

Given that discrimination based on phase matching considerations alone can never provide complete contrast between direct and cascade fifth-order signals, there is the potential for cascade and cascade/direct fifth-order cross-terms to remain in our measured signal. While under perfect phase matching conditions, the direct fifth-order signal field would be 90° phase-shifted from cascade fields, deviation from perfect phase matching produces phase rotation in the signals and allows for the existence of cascade/direct fifth-order cross-terms.^{24,29} Thus we consider both the cascade and the cascade/direct fifth-order cross-terms in detail to account for their potential presence in our measured signal. Using homodyne detection, we measure the intensity of the signal,

$$S(\tau_2, \tau_4) = \int_{-\infty}^{\infty} dt |\epsilon^{(5)}(\tau_2, \tau_4) + \epsilon^{(\text{cas})}(\tau_2, \tau_4)|^2, \quad (13)$$

with

$$\epsilon^{(5)}(\tau_2, \tau_4) = \frac{\omega_s^2}{|k'_s|c^2} NO^{(5)} R^{(5)}(\tau_2, \tau_4) F^{(5)},$$

where $F^{(5)}$ is the single integral in Eq. (5) of the phase matching section. Let us consider the cascade contributions. $\epsilon^{(\text{cas})}$ is the sum of the four cascade signal fields, an example of which was given in Eq. (7). These four cascade signals will contribute both individually and via cross-terms to the total measured intensity. The double integral comprising beam overlap discussed in the phase matching section and present in Eq. (7) is defined as $F^{(\text{cas})}$, and this number is defined for the four possible cascade pathways, giving F_{s1} ,

F_{s2} , F_{p1} , F_{p2} . Combining these elements gives the expression for the measured signal that includes both direct and cascade contributions:

$$\begin{aligned}
S(\tau_2, \tau_4) &= \int_{-\infty}^{\infty} dt |\epsilon^{(5)}(\tau_2, \tau_4) + \epsilon^{(\text{cas})}(\tau_2, \tau_4)|^2 \\
&= \int_{-\infty}^{\infty} dt [O^{(5)2} [A_5^2 N^2 R^{(5)}(\tau_2, \tau_4)^2 |F_5|^2 + A_{s1}^2 A_{s1i}^2 N^4 R_a^2(\tau_2) R_b^2(\tau_4) |F_{s1}|^2 + A_{s2i}^2 N^4 R_c^2(\tau_2) R_d^2(\tau_4) |F_{s2}|^2 \\
&\quad + A_{p1}^2 A_{p1i}^2 N^4 R_e^2(\tau_2 + \tau_4) R_f^2(\tau_4) |F_{p1}|^2 + A_{p2i}^2 N^4 R_g^2(\tau_2 + \tau_4) R_h^2(\tau_4) |F_{p2}|^2 + A_5 A_{s1} A_{s1i} N^3 \\
&\quad \times R^{(5)}(\tau_2, \tau_4) R_a(\tau_2) R_b(\tau_4) [2 \operatorname{Re}(F_{s1}^* F_5)] + A_5 A_{s2} A_{s2i} N^3 R^{(5)}(\tau_2, \tau_4) R_c(\tau_2) R_d(\tau_4) [2 \operatorname{Re}(F_{s2}^* F_5)] \\
&\quad + A_5 A_{p1} A_{p1i} N^3 R^{(5)}(\tau_2, \tau_4) R_e(\tau_2 + \tau_4) R_f(\tau_4) [2 \operatorname{Re}(F_{p1}^* F_5)] + A_5 A_{p2} A_{p2i} N^3 R^{(5)}(\tau_2, \tau_4) R_g(\tau_2 + \tau_4) R_h(\tau_4) \\
&\quad \times [2 \operatorname{Re}(F_{p2}^* F_5)] + A_{s1} A_{s2} A_{s1i} A_{s2i} N^4 R_a(\tau_2) R_b(\tau_4) R_c(\tau_2) R_d(\tau_4) [2 \operatorname{Re}(F_{s1}^* F_{s2})] \\
&\quad + A_{s1} A_{p1} A_{s1i} A_{p1i} N^4 R_a(\tau_2) R_b(\tau_4) R_e(\tau_2 + \tau_4) R_f(\tau_4) [2 \operatorname{Re}(F_{s1}^* F_{p1})] + A_{s1} A_{p2} A_{s1i} A_{p2i} N^4 R_a(\tau_2) R_b(\tau_4) \\
&\quad \times R_g(\tau_2 + \tau_4) R_h(\tau_4) [2 \operatorname{Re}(F_{s1}^* F_{p2})] + A_{s2} A_{p1} A_{s2i} A_{p1i} N^4 R_c(\tau_2) R_d(\tau_4) R_e(\tau_2 + \tau_4) R_f(\tau_4) [2 \operatorname{Re}(F_{s2}^* F_{p1})] \\
&\quad + A_{s2} A_{p2} A_{s2i} A_{p2i} N^4 R_c(\tau_2) R_d(\tau_4) R_g(\tau_2 + \tau_4) R_h(\tau_4) [2 \operatorname{Re}(F_{s2}^* F_{p2})] \\
&\quad + A_{p1} A_{p2} A_{p1i} A_{p2i} N^4 R_e(\tau_2 + \tau_4) R_f(\tau_4) R_g(\tau_2 + \tau_4) R_h(\tau_4) [2 \operatorname{Re}(F_{p1}^* F_{p2})]]]. \tag{14}
\end{aligned}$$

Here,

$$\begin{aligned}
R_a(\tau_2) &= R_{x321}^{(3)}(\tau_2), \quad R_b(\tau_4) = R_{s54x}^{(3)}(\tau_4), \\
R_c(\tau_2) &= R_{x421}^{(3)}(\tau_2), \quad R_d(\tau_4) = R_{s53x}^{(3)}(\tau_4), \\
R_e(\tau_2 + \tau_4) &= R_{sx21}^{(3)}(\tau_2 + \tau_4), \quad R_f(\tau_4) = R_{x543}^{(3)}(\tau_4), \\
R_g(\tau_2 + \tau_4) &= R_{x521}^{(3)}(\tau_2 + \tau_4), \quad R_h(\tau_4) = R_{sx43}^{(3)}(\tau_4),
\end{aligned}$$

where x is the signal field emitted from the first step of the cascade and s is the final signal field. The O factors are those defined in the phase matching section of this paper, as are the F factors. To reiterate, the F factors are

$$\begin{aligned}
F_5 &= \int_0^l dz o^{(5,4,3,2,1)}(z) \exp(i\Delta k \cdot z), \\
F_{s1} &= \int_0^l dz o^{(5,4)}(z) \exp(i\Delta k \cdot z) \\
&\quad \times \int_0^z dz' o^{(3,2,1)}(z') \exp(i\Delta k' \cdot z'), \\
F_{s2} &= \int_0^l dz o^{(5,3)}(z) \exp(i\Delta k \cdot z) \\
&\quad \times \int_0^z dz' o^{(4,2,1)}(z') \exp(i\Delta k' \cdot z'), \\
F_{p1} &= \int_0^l dz o^{(4,3)}(z) \exp(i\Delta k \cdot z) \\
&\quad \times \int_0^z dz' o^{(5,2,1)}(z') \exp(i\Delta k' \cdot z'), \\
F_{p2} &= \int_0^l dz o^{(2,1)}(z) \exp(i\Delta k \cdot z) \\
&\quad \times \int_0^z dz' o^{(5,4,3)}(z') \exp(i\Delta k' \cdot z').
\end{aligned}$$

The factors of A are the $\omega_s^2/|k'_s|c^2$ factors, and there are nine of these. For the overall direct fifth-order process, A_5

$= \omega_{s,s}^2/(|k'_{s,s}|c^2)$ whereas for the first step in the first symmetric cascade, for example, $A_{s1i} = \omega_{s,s1i}^2/(|k'_{s,s1i}|c^2)$ and for the second step in that cascade, $A_{s1} = \omega_{s,s1}^2/(|k'_{s,s1}|c^2)$.

The phase matching numbers (F factors) have been calculated for the geometry that was employed in this paper and in Ref. 29. Again, these numbers are defined above, and the squares of these numbers have units of $\epsilon^{10}l^2$, $\epsilon^{10}l^3$, or $\epsilon^{10}l^4$ with ϵ an electric field and l a length. Of the 15 terms above, 10 are purely cascade contributions, and these have units of $\epsilon^{10}l^4$ for the square of the phase matching factor. The numbers for these contributions are thus directly comparable to each other. Table I presents the F factors for each of these ten contributions. Because each of the F factors is complex, any of the cross-term contributions to the signal can be negative. Table II lists the phase matching numbers for the four

TABLE I. Phase matching terms and factors for the ten pure cascade terms. F_{s1} refers to the phase matching factor associated with the first symmetric cascade ($k_1 - k_2 - k_3$), F_{s2} with the second symmetric cascade ($k_1 - k_2 + k_4$), F_{p1} with the first parallel cascade ($k_1 - k_2 + k_5$), and F_{p2} with the second parallel cascade ($-k_3 + k_4 + k_5$). The phase matching numbers have been calculated numerically according to Eq. (7) and have units of $\epsilon^{10}l^4$. These numbers were used in the simulation of all cascade signals shown in this paper in accordance with Eq. (14).

Phase matching terms	Phase matching factors ($\epsilon^{10}l^4$)
$ F_{s1} ^2$	374
$ F_{s2} ^2$	396
$ F_{p1} ^2$	3220
$ F_{p2} ^2$	3463
$2^* \operatorname{Re}(F_{s1}F_{s2})$	-692
$2^* \operatorname{Re}(F_{s1}F_{p1})$	2133
$2^* \operatorname{Re}(F_{s1}F_{p2})$	2202
$2^* \operatorname{Re}(F_{s2}F_{p1})$	-2204
$2^* \operatorname{Re}(F_{s2}F_{p2})$	-2294
$2^* \operatorname{Re}(F_{p1}F_{p2})$	6676

TABLE II. Phase matching terms and factors for the four cross-terms between the direct fifth-order signal and the cascades present in Eq. (14).

Phase matching terms	Phase matching factors ($\epsilon^{10}l^3$)
$2^* \text{Re}(F_{s1}F_5)$	-4256
$2^* \text{Re}(F_{s2}F_5)$	-3749
$2^* \text{Re}(F_{p1}F_5)$	789
$2^* \text{Re}(F_{p2}F_5)$	1998

terms that are cascade/direct fifth-order cross-terms.

To compare the measured signals to the expected cascade signals, simulations of the cascade signals using third-order measurements in accordance with Eqs. 1(a) and 1(b) are performed. These simulations include all of the cascade terms listed in Table I. In all simulations to be presented in this paper, third-order measurements (Fig. 4) are used as the basis with which to simulate the cascades. Because the total cascade signals are simulated using measured signals, they implicitly include A , N , and O factors (as well as an F factor that in the generally used phase matching formulation would be assumed to be 1 here). The fact that these A , N , and O factors do not have the same values as would those present in a measured cascade signal only introduces an amplitude difference from the true cascade.

C. Relative intensities of the tensor elements

Reference 29 concluded that the R_{zzzzz} signal was dominated by direct fifth-order signal with a small amount of contamination by residual cascade signals, a conclusion supported by work presented in this paper. This will be discussed in much more detail below. Importantly, the fact that the R_{zzzzz} tensor element is dominated by direct fifth-order signal does not necessarily imply that this will be true of other tensor elements collected in the same geometry. This is

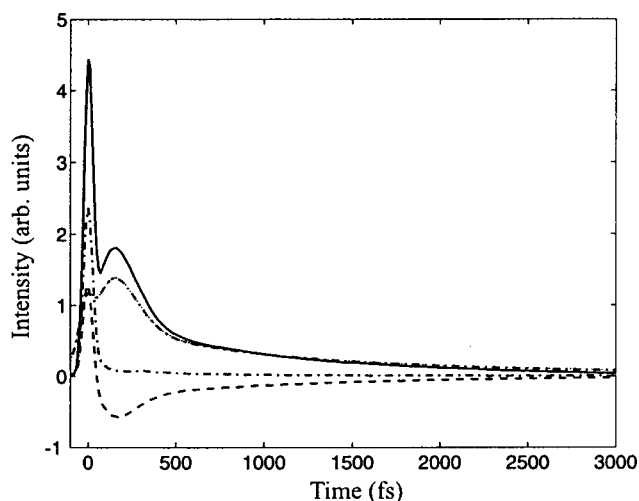


FIG. 4. Third-order data of room temperature CS₂: R_{zzzz} (solid line), R_{yyyz} (dashed line), R_{mmzz} (dash-dot line), and R_{zyyz} (dash-dot-dot line). All data were collected in the heterodyne pump-probe configuration except for the R_{zyyz} data, which were collected in the homodyne "box-car" configuration. The square root of the R_{zyyz} data (arbitrarily scaled to the other data sets) is shown here for comparison with the heterodyne data sets. Similar data were used throughout this paper to simulate the cascade signals according to Eqs. (1a) and (1b).

because different tensor elements of the response are expected to have different magnitudes for the direct fifth-order signal as well as different magnitudes for the third-order signals that comprise the cascades.^{20–22,35,36,41,42} Unlike the R_{zzzzz} signal, which is expected to have a large direct fifth-order signal, certain tensor elements are expected to have small direct fifth-order signals and large third-order signals. Such tensors may still be dominated by, and generally resemble, a cascade signal. This will be discussed further in the following sections in reference to other tensor elements collected. In the only analysis to date of the coherent part of the fifth-order response that includes explicit dependence of the signal on incoming beam polarizations, Murry *et al.* have explored the sizes of the third- and fifth-order polarizability weighted densities of states (PWDOSs), frequency dependent quantities proportional to signal amplitude.^{20–22} They use INM analysis to calculate the PWDOSs for CS₂, and this analysis both predicts the sizes of various tensor elements and shows that polarization selectivity can selectively weight particular Liouville pathways that contribute to the direct fifth-order signal.²¹ The way in which this approach explores polarization selectivity will be discussed in more detail below: here, the expected sizes of the direct fifth-order signal will be discussed.

The contributions to the PWDOSs can be described in terms of three rotationally invariant quantities. To calculate the PWDOS corresponding to a particular tensor element of the direct fifth-order response, Murry, Fourkas, and Keyes (MFK) calculate the appropriate combination of rotational invariants for two interactions via $\alpha^{(1)}$ and one via $\alpha^{(2)}$. The sums of these rotational invariants are then binned according to frequency to create the PWDOS for each tensor element of interest.²¹ An earlier analysis of rotational invariants for the various tensor elements, based on symmetry arguments instead of INM simulations, was also done and reached similar conclusions.²⁰

Before further comparison of experimental data to theoretical predictions is undertaken, it is important to note that MFK make several assumptions in deriving their results. One of these assumptions is that direct fifth-order signal is fully generated through nonlinear polarizability. They justify this based on analysis showing that the rotational invariants contributing to the fifth-order signal generated through anharmonicity would average to near zero.²¹ Even if this is the case, it excludes the impact of anharmonicity-driven relaxation on the shape and decay of the signal. Further, these results do not include mode-coupling ($R^{(5),NP}$ including $\alpha_{ab}^{(2)}$ with $a \neq b$ terms). As will be discussed in relation to the R_{zzzzz} tensor element, while the diagonal terms $\alpha_{aa}^{(2)}$ may dominate, mode-coupling is likely to be important in determining the signal shape and decay at longer times (or lower frequencies), and it is the $\alpha_{ab}^{(2)}$ terms that include the interesting information regarding couplings between nuclear motions. Also, MFK do not fully explore contributions from signals arising from terms dictated by $\alpha^{(2)}\alpha^{(2)}\alpha^{(2)}$ interactions, though they do suggest these should not be very important in many tensor elements. However, more attention to such pathways may be warranted because these terms are likely more important in fifth-order signals than are analogous

terms in third-order signals (signals due to $\alpha^{(2)}\alpha^{(2)}$ interactions), which are generally unimportant even for highly polarizable systems like CS_2 .^{18,20–22}

Within these assumptions, MFK calculate relative intensities of the PWDOSs as a function of frequencies in the range of 0–200 cm^{-1} . Figure 2 of Ref. 21 displays that information. The PWDOSs are calculated for different contributions to the direct fifth-order signal and do not necessarily correspond directly to measured experimental signals. For example, MFK tabulate the PWDOS for direct fifth-order signal due to an $\alpha_{zz}^{(1)}\alpha_{zz}^{(1)}\alpha_{zz}^{(2)}$ set of interactions. This means any signal, regardless of time-ordering, in which the $\alpha^{(2)}$ interaction is induced by a z -polarized pulse pair and two $\alpha^{(1)}$ interactions are induced by z -polarized pulse pairs is included in this PWDOS. In this case, the PWDOS does correspond directly to the measured signal R_{zzzzzz} (given that it is generated solely through nonlinear polarizability). On the other hand, a $\alpha_{zz}^{(1)}\alpha_{zz}^{(1)}\alpha_{yy}^{(2)}$ PWDOS, for example, would correspond to a combination of an R_{yyzzzz} signal and an R_{zzyyzz} signal, since in general the $\alpha_{yy}^{(2)}$ interaction may occur with either the second or third interaction. We have previously mentioned that in certain cases, the two or zero quantum interaction may also occur with the first pulse,^{17,40} and then this PWDOS would also include the R_{zzzyyz} signal.

Looking at the PWDOSs shown in the figures in Ref. 21, we see that $\alpha_{zz}^{(1)}\alpha_{zz}^{(1)}\alpha_{mm}^{(2)}$ has the largest PWDOS. Assuming the $\alpha^{(2)}$ excitation only occurs with the second or third interaction, this PWDOS describes both the R_{mmzzzz} and R_{zzmmzz} signals. The next largest is the $\alpha_{zz}^{(1)}\alpha_{zz}^{(1)}\alpha_{zz}^{(2)}$ PWDOS (R_{zzzzzz}). This is followed closely by $\alpha_{zz}^{(1)}\alpha_{zz}^{(1)}\alpha_{yy}^{(2)}$ (R_{yyzzzz} and R_{zzyyzz}) and $\alpha_{mm}^{(1)}\alpha_{zz}^{(1)}\alpha_{zz}^{(2)}$ (this PWDOS must describe the R_{zzzzmm} signal and describes the R_{zzmmzz} and R_{mmzzzz} signals depending on when the $\alpha^{(2)}$ interaction occurs; R_{zzzzmm} should be a measure of the strength of this PWDOS²¹). Next is the $\alpha_{zy}^{(1)}\alpha_{zy}^{(1)}\alpha_{zz}^{(2)}$ PWDOS (R_{zzzyyz} and R_{zyzzzy}). Then comes the $\alpha_{yy}^{(1)}\alpha_{zz}^{(1)}\alpha_{zz}^{(2)}$ PWDOS (necessarily R_{zzzyyz}), which is actually negative, a property unseen in any third-order PWDOS calculation. Finally comes $\alpha_{zz}^{(1)}\alpha_{zy}^{(1)}\alpha_{zy}^{(2)}$ (necessarily R_{zyzyzz}), which is very small in magnitude over the entire frequency range calculated. Figure 8 of reference 21 shows the third-order PWDOSs that would act to create the cascade contributions in each of the measured tensor elements. The one notable feature of these calculations with respect to our measurements is that the third-order magic angle PWDOS is much smaller than the polarized one (R_{zzmm} and R_{mmzz} vs R_{zzzz}). This is already well known from third-order spectroscopic^{41–45} and theoretical^{35,36,46} results, which show that by symmetry this signal will be zero at times corresponding to reorientational diffusive motions. This suggests that the magic angle direct fifth-order signals, R_{zzmmzz} , R_{mmzzzz} , and R_{zzzzmm} , have the greatest ability to select against any residual cascade present in the signals measured in the geometry used here.

The measured intensities of the fifth-order signals do not in all cases agree with the predicted intensities of MFK, although again a direct comparison of most of the tensor elements is impossible based on the one dimensionality of the PWDOSs and their inclusion of all time-orderings. Because the time-dependence of the various measured tensor ele-

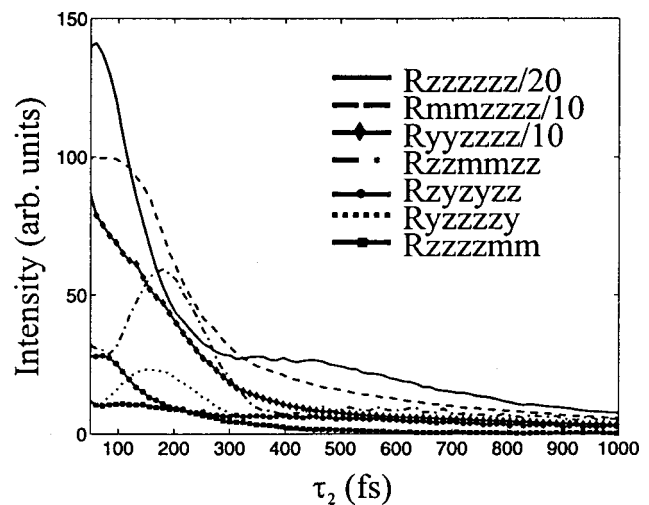


FIG. 5. Slices at $\tau_4=180$ fs for the different polarization tensors. As indicated in the legend, slices have been scaled so as to be more easily viewed.

ments of the signal vary so greatly, to choose any one point at which to compare signal intensities is misleading. The relative measured signal intensity is judged by taking slices along τ_2 at $\tau_4=180$ fs (Fig. 5). These slices were taken consecutively, varying the polarizations of the incoming beams and the polarization selection for the signal. All signals were polarization-selected except the R_{mmzzzz} signal. Its actual intensity compared to the other tensor elements was evaluated by subsequent measurements of an R_{zzzzzz} signal with and without a polarizer cube. In general terms, judging by the slices measured at $\tau_4=180$ fs, R_{zzzzzz} is the most intense signal. The R_{mmzzzz} signal is next in intensity, followed by the R_{yyzzzz} signal. A moderately steep drop-off in intensity is seen between that tensor element and the one next highest in signal intensity, the R_{zzmmzz} signal. Following this are the R_{zyzzzy} , R_{zyzyzz} , and R_{zzzzmm} signals.

While the R_{zzzzzz} signal is certainly the most intense one measured, it is predicted to be the second or third largest based on the rotational invariant analysis of MFK. This may be evidence that residual cascade and/or cascade/direct fifth-order terms are present in this measured tensor element whereas this is likely untrue of some of the other tensor elements studied. The R_{mmzzzz} signal is rather intense, as predicted by the PWDOS calculations. The R_{zzmmzz} signal is less so, but still at a substantial level compared to the smallest tensor elements collected. The R_{zzzzmm} signal is much smaller than the other magic angle signals, also in agreement with the calculated PWDOSs. None of these signals is expected to have significant residual cascade contributions, as discussed above. The R_{yyzzzz} signal is quite large, also in agreement with calculations. The sizes of the three least intense tensor elements collected (the R_{zyzzzy} , R_{zyzyzz} , and R_{zzzzmm} signals, in order of decreasing intensity) are not in complete agreement with calculations. Calculations suggest the order would be R_{zzzzmm} , R_{zyzzzy} , and R_{zyzyzz} in order of decreasing intensity. The deviations in sizes are small in these cases, and any number of small failures of the assumptions made in the calculations of MFK could account for the differences between simulations and experiment. Further, re-

producibility of the data for the least intense tensor elements collected is imperfect. Small differences in alignment allow for different amounts of cascade signals to be present in the measured signals. In addition, incomplete elimination of third-order signals that emerge in a number of directions (as determined by any three of the incoming beams' wave vectors) and may scatter into the direction of the desired signal allows for heterodyning of the measured fifth-order signal with small amounts of these scattered third-order signals, also potentially changing the measured intensities of the signals.

D. The R_{zzzzzz} tensor element

Figure 6(a) presents the measured R_{zzzzzz} signal. Figure 6(b) shows the results of the total cascade simulation for the R_{zzzzzz} tensor element. As mentioned above, the simulations were performed using third-order measurements in accordance with Eqs. 1(a) and 1(b) and the phase matching values given in Table I [in conjunction with Eq. (14)]. Figure 6(c) shows the measured signal with the total cascade simulation removed. This subtraction was performed assuming that signal at $\tau_2 = 1200$ fs, $\tau_4 = 100$ fs [signal of intensity corresponding to the last contour present in Fig. 6(a)] is attributable to residual cascades: this is based on arguments presented in Ref. 29. The cascade simulation is then scaled to this point and subtracted from the measured signal, leaving the data displayed in Fig. 6(c). Slices from the R_{zzzzzz} measured surface, the simulated cascade surface, and the measured surface from which the cascades have been removed are shown in Fig. 6(d). These slices were taken at $\tau_4 = 100$ fs, close to where both the measured and simulated surfaces peak along that dimension. The slices are presented from 50 fs onward because the simulation in Fig. 6(b) does not include the contribution around time zero from the cascade terms that contribute to the back quadrant of the signal (where pulses three and four precede pulses one and two). The contribution in the back quadrant is different from that in the front quadrant, unlike in Ref. 25, because the phase matching geometry used here is not symmetric. The most notable difference between the simulated cascade signal and the measured R_{zzzzzz} signal (as well as the signal with the suspected residual cascade subtracted) is that the simulated cascade signal decays much more slowly than does the measured signal along the τ_2 dimension. This is also true for the decay of these signals along τ_4 . These differences in decay time scales suggest that there is not much contribution of the cascades to the measured signal. These differences could also suggest that the remaining cross-terms, those between the direct fifth-order signal and the cascades, contribute in a negative manner and thus alter the time scale of the decay. We will discuss below why this possibility is not expected to be important here.

Table II presents the phase matching numbers for the cascade/direct fifth-order cross-terms. There are two negative terms, the cross-terms between the symmetric cascades and the direct fifth-order signal. The numbers presented in Table II show that in the R_{zzzzzz} signal (in which all cascades are comprised of R_{zzzz} third-order signals) contributions from

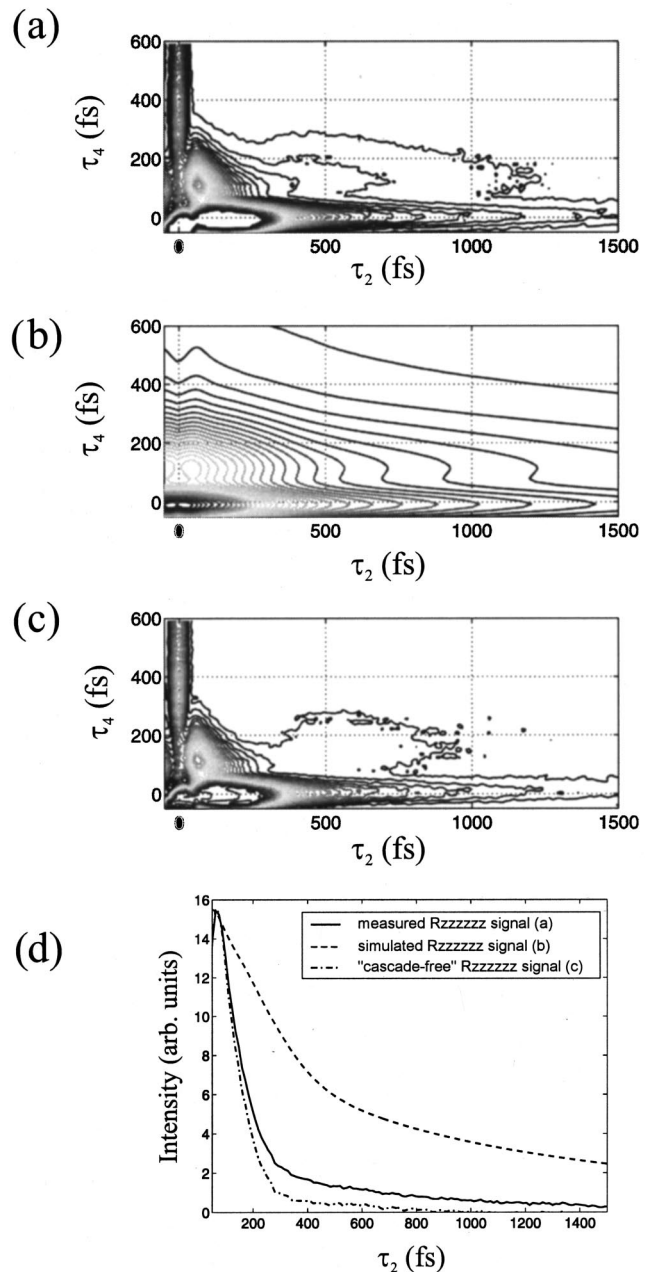


FIG. 6. (a) Contour plot of the R_{zzzzzz} tensor element shown to longer times in τ_2 than as presented in Fig. 2(a). (b) Simulation of cascade terms present in Eq. (14) with intensities given in Table I for the R_{zzzzzz} tensor element. (c) Contour plot of the R_{zzzzzz} signal when the simulation in (b) is scaled to the last visible contour in (a) and then subtracted from the measured signal. (d) Slices from the three contour plots above at $\tau_4 = 100$ fs. The slices have been scaled so that they have approximately equal intensity at their peaks: this highlights the similarity in the time dependencies of the measured and corrected signals and their distinct difference from the time dependence of the cascade signal.

the symmetric cascade/direct fifth-order cross-terms will be more important than those from the parallel cascade/direct fifth-order cross-terms. Here, we assume that the fifth-order signal (the shape of which is *a priori* unknown) will be rather symmetric with respect to the two time axes, which seems to be a reasonable assumption based on INM, QNM, and MD simulations. Then, among the cascade/direct fifth-order cross-terms, the major contribution to the measured

signal would be a symmetric signal that is negative in amplitude with respect to the pure cascade terms (with intensities given in Table I) and the direct fifth-order signal. We see no evidence for symmetric residual contributions in the measured signal at long times, where the signal dies off significantly slower along τ_2 than along τ_4 . If these symmetric cascade/direct fifth-order cross-terms contributed significantly, they would subtract from the direct fifth-order signal and any residual pure cascade terms, and we may expect to see an extension along the τ_4 axis instead of the τ_2 axis where it is present. This is because the contribution from the pure cascade terms and the parallel cascade/direct fifth-order cross-terms would add positively to the direct fifth-order signal, resulting in an extension along τ_2 . Then, subtracting the symmetric cascade/direct fifth-order terms from this signal would result in both a negative dip along τ_4 at times longer than the direct fifth-order signal extends and a decrease in signal magnitude along τ_2 . Homodyne detection of such a signal would result in a measured response extended along the τ_4 dimension or symmetric with respect to τ_2 and τ_4 , depending on how large the symmetric cascade/direct fifth-order terms were. So, the extension of the measured signal along τ_2 as well as the similarity in peak positions in Figs. 6(a) and 6(b) suggest that it is indeed pure cascade terms and not cascade/direct fifth-order cross-terms that contribute to the probable residual cascades in the measured signal. Additionally, as seen in Table I, the symmetric/parallel cascade-cascade cross-terms largely cancel out in the case of the R_{zzzzzz} signal (in which the only third-order signal that contributes to the cascades is the R_{zzzz} tensor element), leaving the pure parallel cascades and the parallel/parallel cascade cross-term the dominant terms in the residual cascade. Of course, as shown in Figs. 6(c) and 6(d), even these contributions appear to contribute only very minimally to the measured signal.

Our results showing that direct fifth-order signal dominates cascade signals in this geometry disagree in a quantitative sense with recent calculations by Jansen *et al.*⁴⁷ They calculate that the intensity of the cascade signal compared to the direct fifth-order signal is $\sim 4 \times 10^6$ when using 620 nm light. For our 800 nm light, the ratio would be $\sim 2.4 \times 10^6$. Such a ratio would necessitate a ratio of at least 10^6 in the squared phase matching factors for the direct fifth-order signal to effectively compete with the cascade signals. Our cascade phase matching factors are given in Table I. Our direct fifth-order squared phase matching factor [the integral in Eq. (5)] is $3.2 \times 10^5 \epsilon^{10} l^2$. So, we have a ratio of only $10^2 - 10^3$ in the squared phase matching factors for the direct fifth-order and cascade signals: however, we believe we do see predominantly direct fifth-order signal. One important factor that may contribute to this discrepancy is that Jansen *et al.* do not account for local field effects and thus only account for single molecule motions: while it has been suggested that single molecule motions are important in third-order spectroscopies, they are suspected to be much less important than collision-induced terms (and molecular/collision-induced cross-terms) in fifth-order spectroscopies.²⁰⁻²² Further, the ratio of the third-order response functions (which participate in the cascades) to the fifth-order response function was es-

timated from the peak values of the third- and fifth-order anisotropies as calculated with a finite field nonequilibrium MD method. The third-order peak value is approximately three orders of magnitude greater than the fifth-order peak value. However, typical values of the ratio of $\alpha^{(2)}$ to $\alpha^{(1)}\alpha^{(1)}$, the ratio of polarizability derivatives that determine the difference in response functions between the nonlinear polarizability generated direct fifth-order signal and the cascade signals, are randomly distributed but appear closer to two orders of magnitude different.²² Such discrepancies could make up the difference between the predicted necessary phase mismatch for the cascades of Jansen *et al.* and our experimental evidence showing that a $10^2 - 10^3$ difference in squared phase matching factors is sufficient to produce a signal dominated by the direct fifth-order response.

So, we believe the R_{zzzzzz} signal to be dominated by direct fifth-order signal, with a small amount of contamination by pure parallel cascade terms, and this contamination is likely evident only in the final one or two contours along τ_2 visible in Fig. 6(a). Thus when comparing to QNM, INM, and MD simulations of the R_{zzzzzz} tensor element, we assume our measured data is dominated by the direct fifth-order signal and directly compare our results to simulations. We have previously reported qualitative agreement with the QNM simulations that include damping. We have phenomenologically associated this damping with anharmonicity, which can both give rise to fifth-order signal and contribute to its rapid decay.²⁹ In addition, we now report agreement with preliminary MD simulations performed by Stratt and co-worker.⁴⁸ While these simulations are for an atomic liquid, there is qualitative agreement in both the shape and time scales between the calculated and measured signals. The MD simulations for the R_{zzzzzz} tensor element produce a signal that peaks at $\tau_2 \sim 20$ fs, $\tau_4 \sim 300$ fs. It extends to ~ 400 fs along τ_2 and ~ 1 ps along τ_4 : this extension along the τ_4 axis is in general agreement with the R_{zzzzzz} signal when given the considerations for cascade contributions mentioned above. Both the simulated and experimental signal are flat along the anti-diagonal ($\tau_2 + \tau_4 = \text{constant}$) and do not exhibit significant echo-like behavior (signal along $\tau_2 = \tau_4$).

Stratt and co-worker also perform an INM calculation for the atomic liquid and compare it to the MD results. The INM simulation indicates that for atomic liquids the $\alpha_{ab}^{(2)}$ term is largely diagonal in the mode index, which results in a strong, long-lived echo-ridge that peaks at $\tau_2 \sim 1$ ps, $\tau_4 \sim 1$ ps. The MD simulations, which unlike the INMs include anharmonicity, die off much more quickly. The conclusion is in agreement with the one drawn earlier from comparison of our data to the QNM simulations by Saito and Ohmine: anharmonicity plays a large role in determining the shape and time scale of decay of the polarized fifth-order signal.^{18,29} However, the importance of anharmonicity may be less obvious in the case of molecular liquids where $\alpha_{ab}^{(2)}$ with $a \neq b$ may become more significant, as not only intermolecular distance but also orientation will determine the magnitude of $\alpha_{ab}^{(2)}$ in molecular liquids. This is also in agreement with the INM and QNM simulations (done for CS₂) of Saito and Ohmine, which do decay much more quickly than those of Stratt, but only when the $a \neq b$ mode coupling is included.

However, in those simulations the $\alpha_{ab}^{(2)} = \alpha_a^{(1)}\alpha_b^{(1)}$ assumption is used: this has been shown to be invalid but may still produce a qualitative picture of how mode-coupling affects the fifth-order signal.^{18,22,29} Thus the rapid decay of the experimental fifth-order signal of CS₂ may arise as much from these nonlinear polarizability induced mode–mode couplings as from anharmonicity. Given this, the type of anharmonicity (diagonal vs off-diagonal in the mode index) found in the MD simulations of atomic liquids may be more applicable to molecular liquids than the magnitude of anharmonicity found in such simulations. In preliminary work, Stratt and co-worker have found that $g_{abc}^{(3)}$ is largely dominated by diagonal terms ($a=b=c$). However, in analogy with the off-diagonal coupling terms in the signal generated through nonlinear polarizability, it may be found that off-diagonal terms of the anharmonicity will also be very important in the decay of the signal.

Previously the characteristics of the direct fifth-order signal were only discussed in the fully two-dimensional area ($\tau_2 > 0$ fs, $\tau_4 > 0$ fs). Here, however, we note the distinct extension along the $\tau_2 = 0$ fs axis present in the measured R_{zzzzzz} signal and not present in measured cascade signals. This extension may arise in part from direct fifth-order signals probing population dynamics that can occur along that dimension.¹⁷ Steffen and Duppen have discussed in detail the direct fifth-order signal described by Eq. (8a) that can be produced along the $\tau_2 = 0$ fs axis, where a hyperpolarizability signal described by Eq. (8b) may also reside. [Such pathways can be seen in Feynman diagrams such as the one shown in Fig. 9(c)]. Here, the first two sets of pulses are overlapped, and this gives a Liouville pathway in which the system evolves in a population state, or a diagonal element of the density matrix, during the second variable time interval. Thus the extended features seen along the $\tau_2 = 0$ fs axis in the R_{zzzzzz} signal and many other tensor elements may reflect population dynamics along this axis. In the absence of hyperpolarizabilities and residual cascade signals, the signal on the $\tau_2 = 0$ fs axis is a direct measure of population dynamics, whereas a slice taken at a given nonzero value of τ_4 along τ_2 is a direct measure of pure dephasing. In the case of the R_{zzzzzz} tensor element, the cascade simulation (which includes the pure cascade terms expected to contribute more substantially to any residual cascade signal than the cascade/direct fifth-order cross-terms) does not have significant signal along the $\tau_2 = 0$ fs axis [Fig. 6(b)]. Thus cascades are expected to contribute very minimally along the $\tau_2 = 0$ fs axis; however, a hyperpolarizability signal governed by Eq. (8b) may contribute there, although its expected intensity is *a priori* unknown. The slow decay of the signal along this axis suggests that we are indeed seeing evidence of direct fifth-order signal that reflects population dynamics along this axis. This will be discussed in more detail for other tensor elements that show a distinct tendency to either select or deselect for these types of Liouville pathways.

E. Magic angle signals

Polarization selectivity has long been used to select for certain dynamics. For example, it is well known that the

magic angle response function, $R_{mmzz}(t) = R_{zzzz}(t) + 2R_{yyzz}(t)$, with one pulse pair set at an angle of 54.7° relative to the other pulse pair, probes only the isotropic response of a liquid.^{36,46} It also has been suggested that information about the response coming from $\alpha^{(2)}\alpha^{(2)}$ type interactions may be accessible by measurements of $R_{mmzz}(t)$.²⁰ The number of beams involved in a fifth-order experiment and the requirement for an $\alpha^{(2)}$ interaction (as induced by nonlinear polarizability for the analysis presented here) for generation of any fifth-order signal, allows for a greater range of polarization selectivity in fifth-order experiments than in third-order ones. This selectivity provides the potential to give different weightings to different Liouville pathways and dynamic behaviors and can be achieved by changing the polarizations of the incoming beams.

Echolike pathways necessarily contain a two quantum interaction in the second step.^{12,20} Using the calculations of MFK to selectively weight for the echo, the tensor element in which the desired pathways are dominated by the largest rotational invariant and the undesired pathways are dominated by the smallest rotational invariant is the one that should be measured. MFK attempt to identify such tensors by varying the polarizations of the pulse pair for which the $\alpha^{(2)}$ interaction is desired: in the case of the echolike pathways this is, as mentioned, the second pulse pair. This can be understood by reference to the Feynman diagram in Fig. 1(b). In this diagram, the first coherence excited is that between the ground and first excited vibrational levels of the probed oscillator or coupled oscillators. The coherence to which this superposition state is transferred upon arrival of the second pulse pair is a coherence between the first and second excited vibrational levels of the probed oscillator(s). For a nearly harmonic case, in which the energy difference between the first two vibrational levels is nearly equal to that between the second and third vibrational levels, this diagram looks like a rephasing diagram used to describe photon echoes. The energy differences of the two superposition states excited are nearly equal in magnitude but opposite in sign, so that when the second coherence is excited, the dynamics of the first coherence period are reversed, potentially allowing for rephasing and the formation of an echo. In the two-dimensional experiment this echo would appear along the diagonal, $\tau_2 = \tau_4$. All echolike signals that can be obtained in the two-dimensional Raman measurement have the $\alpha^{(2)}$ interaction producing a two quantum interaction in the second step, as in the Feynman diagram displayed in Fig. 1(b).

The least effective way to select for the echo or any specific pathway is to measure the R_{zzzzzz} signal: this measurement always includes two $\alpha_{zz}^{(1)}$ interactions and one $\alpha_{zz}^{(2)}$ interaction, thus weighting all pathways equally (now the subscripts indicating polarizations of the incoming pulse pairs have been explicitly included).²¹ On the other hand, MFK have suggested several tensor elements that will heavily weight Liouville pathways where the $\alpha^{(2)}$ interaction comes second. These tensor elements will weight for the echo pathways. Of the suggested tensor elements, R_{zzmmzz} is the most promising for our experiment: because the third-order response R_{mmzz} is very small, any cascade contributions to the fifth-order signal will be very weak, even com-

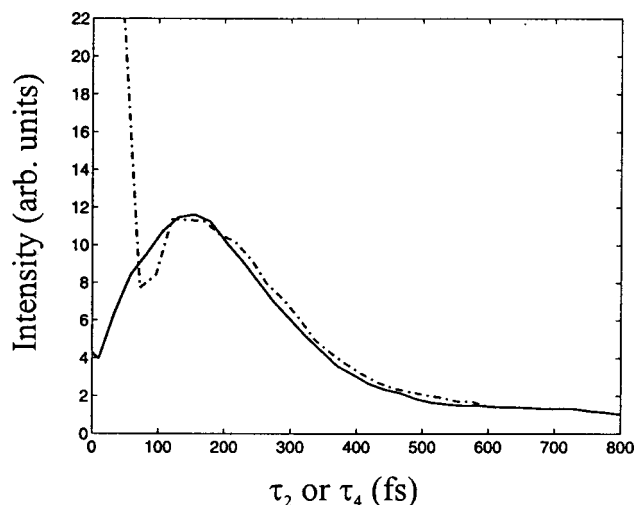


FIG. 7. Slices from the measured signal shown in Fig. 3(b) (R_{zzmmzz}). The solid line is the data along $\tau_4 = 180$ fs. The dashed line is that along $\tau_2 = 180$ fs.

pared to the very small contributions evident in the R_{zzzzzz} signal. Significantly, as mentioned above, this tensor element is expected to have the largest direct fifth-order signal of any of the tensor elements studied by MFK. In addition, the R_{mmzz} signal reflects only isotropic dynamics and therefore contains none of the long-time anisotropic reorientational dynamics seen in other third-order signals.^{36,46} Conversely, any fifth-order tensor element with a pair of pulses set at the magic angle need not exclude diffusive motions based on symmetry arguments alone, as no fifth-order tensor elements are purely isotropic.^{20,21,38,49} The presence of any longer time components in these signals then can not be attributed to cascades and can provide valuable insight into which dynamics the fifth-order experiment can probe.

The R_{zzmmzz} signal is presented in Fig. 3(b). The peak of the signal is at $\tau_2 \sim 150$ fs and $\tau_4 \sim 150$ fs, and the signal is fairly symmetric with a slightly slower decay along τ_4 than along τ_2 . The signal extends in each direction well beyond 600 fs as can be seen in slices shown in Fig. 7. While we might reasonably expect some discrimination against anisotropic behavior in the magic angle signals through analogy with third-order magic angle signals, the long time behavior in this tensor element is striking and suggests that this is not the case. Here, we concentrate on the response in the purely two-dimensional area ($\tau_2 > 0$ fs, $\tau_4 > 0$ fs) since this is where rephasing dynamics would be manifest. Compared to the R_{zzzzzz} signal, there is a significantly slower decay along both dimensions and along the diagonal ($\tau_2 = \tau_4$), where echolike behavior would appear. Diagonal slices from the R_{zzzzzz} and R_{zzmmzz} surfaces are shown in Fig. 8(b). Clearly the echolike signal extends to longer time in the R_{zzmmzz} signal. However, as concluded in a previous paper, which showed a diagonal slice from the R_{zzzzmm} signal, another tensor element that was suggested to weight for the echo,²¹ the time scale of rephasing is comparable to that of the inverse frequencies of the modes being probed, and thus the liquid is well-described as homogeneous.²⁹ Of course, because the damping of the signal can be due to both anharmonicity and pure dephasing,

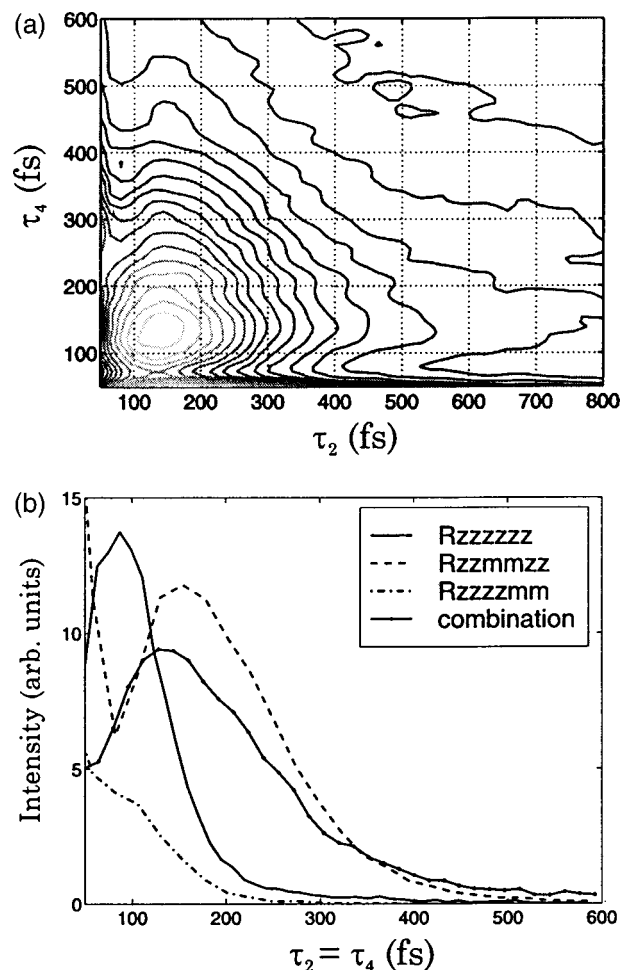


FIG. 8. (a) Contour plot of the combined magic angle surface (presented as the square of the response so that it is directly comparable to the measured homodyne signals) that isolates the contribution from terms with the polarization derivative $\alpha_{zz}^{(1)}\alpha_{mm}^{(2)}\alpha_{zz}^{(1)}$. (b) Diagonal slices from the R_{zzzzzz} (solid line), R_{zzmmzz} (dashed line), R_{zzzzmm} (dot-dash line), and the combination surface presented in (a) (line with cross markers). Note the peaks of the R_{zzmmzz} and combination diagonal slices occur significantly later than those of either of the other two slices.

a diagonal slice only provides a lower limit on the inhomogeneity of the sample, not an absolute value.

Following the suggestion of Murry *et al.*, the magic angle responses have been summed in a particular manner in order to compare our data directly to their PWDOS calculations.²¹ While this procedure was originally suggested for the tensor elements consisting of y and z polarizations, we perform it on the magic angle signals where cascade remnants are much less of a concern. Such an addition procedure is performed assuming pathways with an $\alpha^{(2)}$ interaction in the first step do not contribute to the signal.^{12,20} While this assumption has been used previously, it has been shown to be inexact for systems with either non-Markovian system-bath fluctuations or systems with level dependent vibrational dephasing.^{17,40} The addition procedure is as follows: add together the R_{zzmmzz} and R_{mmzzzz} signals and subtract the R_{zzzzmm} signal from this sum. The relative magnitudes and scaling of the surfaces used are taken from the slices presented in Fig. 5. The three measured magic angle signals are shown in Fig. 3. The combined surface and diagonal slices

through two of the magic angle surfaces are shown in Figs. 8(a) and 8(b).

The combined surface reflects the size of the $\alpha_{zz}^{(1)}\alpha_{zz}^{(1)}\alpha_{mm}^{(2)}$ PWDOS and can be compared directly to the size of the $\alpha_{mm}^{(1)}\alpha_{zz}^{(1)}\alpha_{zz}^{(2)}$ PWDOS and moreover can be compared directly to Fig. 2(d) of Ref. 21. If we assume that the $\alpha^{(2)}$ interaction comes in one of the final two steps of the experiment, the combined surface reflects the size of $\alpha_{zz}^{(1)}\alpha_{zz}^{(1)}\alpha_{mm}^{(2)}$ because the R_{zzmmzz} signal has an $\alpha^{(2)}$ interaction induced by either a zz or an mm pair, as does the R_{mmzzzz} signal, whereas the R_{zzzzmm} signal necessarily has the $\alpha^{(2)}$ interaction originating from a z -polarized pair of pulses. The addition/subtraction procedure then leaves the $\alpha^{(2)}$ interaction necessarily induced by an mm pulse pair, whereas the R_{zzzzmm} signal has the $\alpha^{(2)}$ interaction necessarily generated by a zz pulse pair. The comparison of the diagonal slices in Fig. 8(b) is consistent with several of the observations made by MFK in conjunction with their generation of the $\alpha_{mm}^{(1)}\alpha_{zz}^{(1)}\alpha_{zz}^{(2)}$ and $\alpha_{zz}^{(1)}\alpha_{zz}^{(1)}\alpha_{mm}^{(2)}$ PWDOSs shown in Fig. 2(d) of Ref. 21. First, comparing the diagonal slice from the combined surface to that of the R_{zzmmzz} slice shows that the R_{zzmmzz} slice peaks at ~ 160 fs whereas that of the combined surface peaks closer to 130 fs. This de-emphasis on the echo is expected, as the combined surface equally weights those signals with the m -polarized pulse pair second and third, whereas the R_{zzmmzz} is chosen in an attempt to more heavily weight the signal with the $\alpha_{mm}^{(2)}$ term second. Further, the comparison between the diagonal slice from the R_{zzzzmm} surface and that of the combined surface shows that the combined surface is larger than the R_{zzzzmm} surface as predicted by Fig. 2(d) of Ref. 21. Also, the combined surface weights slower, or lower frequency, motions more heavily than does the R_{zzzzmm} surface. This is also in agreement with the MFK calculations.

F. Semi-polarized signals

While the magic angle signals provide both the ability to detect a direct fifth-order signal unblemished by cascade contributions and potential selection for echolike pathways, some of the semi-polarized measured signals also appear to differently weight select Liouville pathways. Here, however, they appear to preferentially select or deselect for pathways in which the system is in a diagonal state during at least part of the second time period. In the discussion of the R_{zzzzzz} tensor element, the presence of such pathways has already been mentioned: here, we discuss these pathways in more detail. The pathway discussed in reference to the R_{zzzzzz} tensor element is shown in Fig. 9(c). The signal this Feynman diagram depicts is generated through the three-point polarizability correlation function in Eq. (8d) and contributes on the $\tau_2=0$ fs axis. This Feynman diagram shows that the signal along the $\tau_2=0$ fs axis measures population dynamics, assuming hyperpolarizability and residual cascade signals are not present. Now, however, we also consider pathways that contribute in the $\tau_2>0$ fs, $\tau_4>0$ fs area. Two types of diagrams, which will be discussed in more detail below, that depict signals that give rise to population dynamics in this area are shown in Figs. 9(d) and 9(e). Murry, Fourkas, and

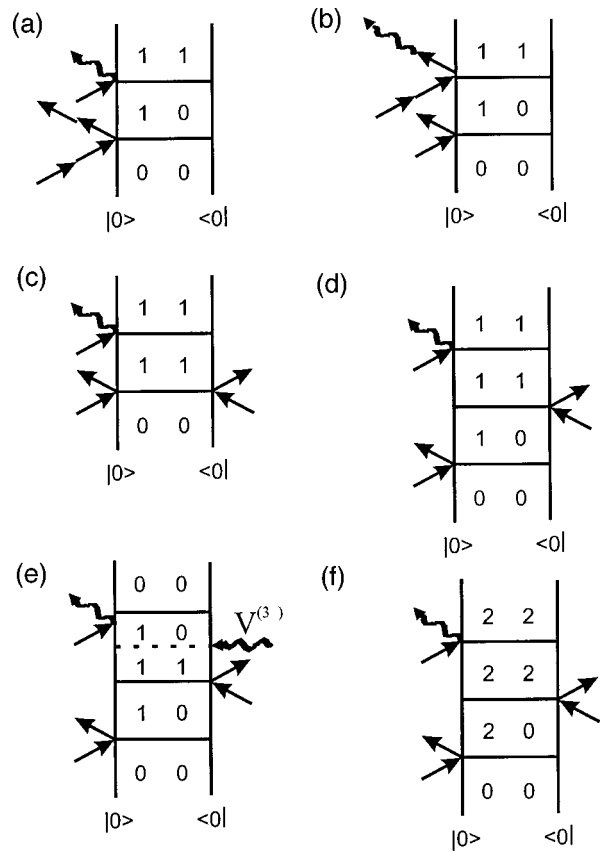


FIG. 9. Several double sided Feynman diagrams that depict pathways important in the measured signals. (a) A hyperpolarizability pathway described by Eq. (8b) and potentially appearing on the $\tau_2=0$ fs axis. (b) A hyperpolarizability pathway described by Eq. (8c) and potentially appearing on the $\tau_4=0$ fs axis. (c) A direct fifth-order signal pathway described by Eq. (8d) and potentially appearing on the $\tau_2=0$ fs axis. It includes population dynamics along τ_4 . (d) A direct fifth-order signal pathway described by Eq. (8d) that is generated through nonlinear polarizability terms and includes population dynamics. (e) A direct fifth-order signal pathway described by Eq. (8d) and generated through anharmonicity. It also includes population dynamics. (f) A direct fifth-order signal pathway described by Eq. (8d) and generated through nonlinear polarizability allowed $\alpha^{(2)}\alpha^{(2)}\alpha^{(2)}$ terms.

Keyes discuss such pathways, many of which have a zero quantum interaction occurring in the third step, less directly than they discuss the echolike pathways. In this case, our observations do not completely agree with their suggestions. As mentioned previously, the two surfaces that will be discussed for their apparent potential to select or deselect for population dynamics are the R_{yyzzzz} and R_{yzzzyy} surfaces shown in Figs. 2(c) and 2(d), respectively. First, because according to the PWDOS calculations of MFK, these direct fifth-order signals are smaller than any of those previously discussed, the potential cascade contributions to these signals will be considered.

As discussed in the relative intensities section of this discussion, the R_{mmzzzz} and R_{zzmmzz} tensor elements have the largest PWDOSs for the frequency range probed in this experiment. The R_{zzzzzz} signal has the next-largest PWDOS. Other tensor elements have somewhat smaller PWDOSs, with that corresponding to the R_{zyzyzz} signal very small in magnitude over the entire frequency range calculated. As mentioned previously, the R_{zyzyzz} signal was among the least

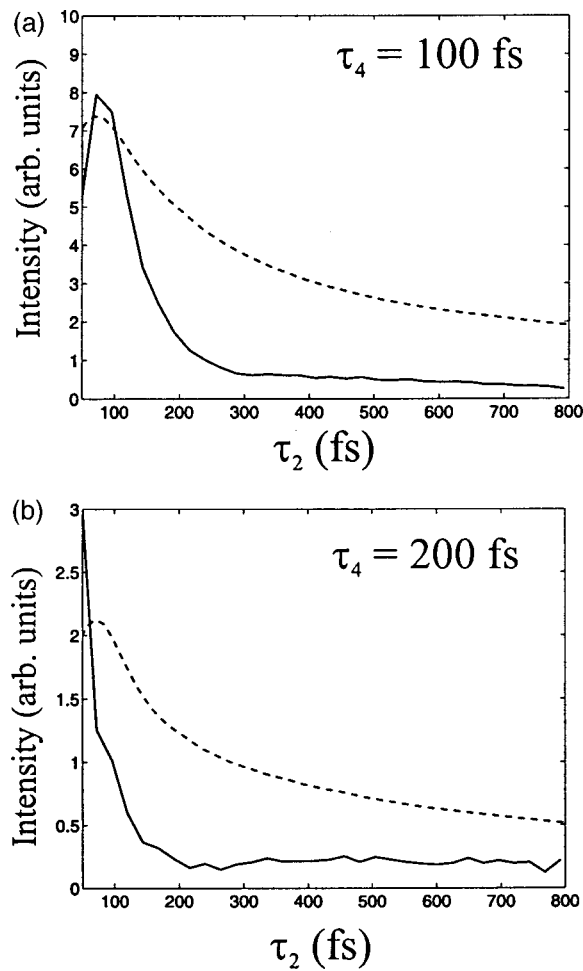


FIG. 10. Slices from the R_{zyzyzz} signal shown in Fig. 2(b) compared to cascades simulated according to Eqs. (1a) and (1b) and amplitudes given in Table I. In both cases the measured signal is given by the solid line and the cascade simulation is given by the dashed line. (a) Slices at $\tau_4 = 100$ fs. (b) Slices at $\tau_4 = 200$ fs.

intense signals collected. It is presented in Fig. 2(b). Figures 10(a) and 10(b) show slices from the measured signal and the full cascade simulation at $\tau_4 = 100$ fs [Fig. 10(a)], close to where both the measured and simulated signals peak, and $\tau_4 = 200$ fs [Fig. 10(b)], at which point the measured signal has mostly decayed and the simulated signal has a dip between two extended features along τ_2 . Figures 10(a) and 10(b) show that the slices from the full cascade simulation decay much more slowly than do those from the measured signal. This strongly suggests that even though the R_{zyzyzz} direct fifth-order signal is expected to be very small, the measured signal is not dominated by pure cascade contributions. Since we have no *a priori* reason to believe this tensor element of the direct fifth-order signal should be symmetric with respect to the two time variables and no simulations to suggest this is a good assumption, we can not conclude cascade/direct fifth-order cross-terms are negligible through examination of the shape of the measured signal. However, the suspected overall small size of the cascades compared to the direct fifth-order signal does suggest that this tensor element has only minimal contributions from cascade/direct fifth-order cross-terms. The fact the direct fifth-order signal

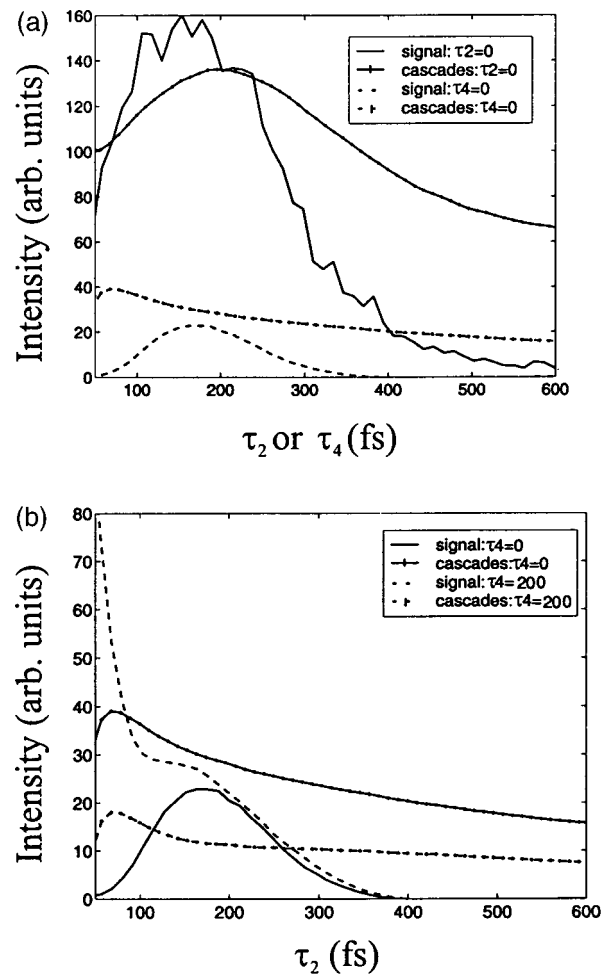


FIG. 11. Slices from the R_{yyzzzz} signal shown in Fig. 2(c). (a) Slices from the measured signal (lines) and cascade (lines with plus markers) at $\tau_2 = 0$ fs (solid lines) and at $\tau_4 = 0$ fs (dashed lines): both cascade slices decay much more slowly than the measured signal slices. (b) Slices from the measured signal (lines) and cascade (lines with plus markers) at $\tau_4 = 0$ fs (solid lines) and at $\tau_4 = 200$ fs (dashed lines): both signal slices decay on the same time scale and much more slowly than the cascades decay.

still appears to be larger than the cascade and cascade/direct fifth-order contributions bodes well for the phase matching discrimination achieved in this geometry and strongly suggests that the other tensor elements measured are also dominated by direct fifth-order signal. Two such signals collected are the R_{yyzzzz} and R_{yzzzyy} tensor elements. Both tensor elements are expected to have larger direct fifth-order signals than the R_{zyzyzz} tensor element discussed above.²¹ The time-dependence of the R_{yyzzzz} signal [Figs. 11(a) and 11(b)] and the time-dependence and the shape of the R_{yzzzyy} signal [Fig. 12(a)] do not resemble those of the respective cascade simulations. The R_{yzzzyy} signal seems to selectively weight Liouville pathways including population dynamics while the R_{yyzzzz} signal seems to deselect for these pathways, and this will be discussed further below.

Steffen and Duppen have discussed in detail the direct fifth-order signal that can be produced along the $\tau_2 = 0$ fs axis, shown in Fig. 9(c).¹⁷ Here, the first two sets of pulses are overlapped, and this gives a Liouville pathway in which the time evolution is in a population state. Thus the extended

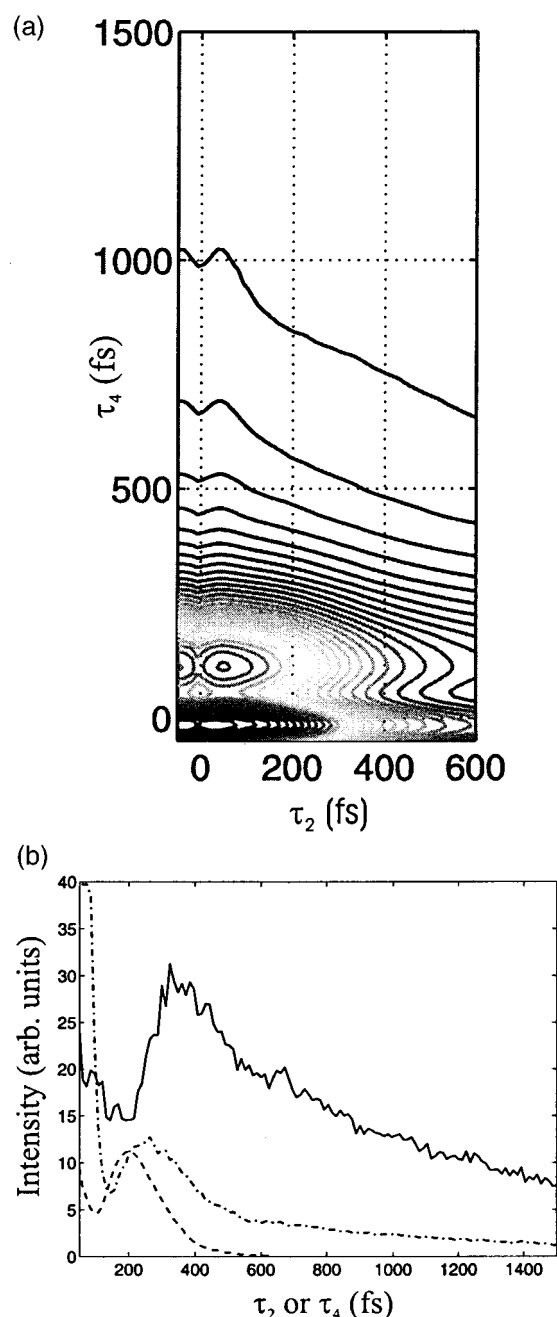


FIG. 12. (a) Cascade simulation of the R_{yzzzz} tensor element. (b) Slices from the measured R_{yzzzz} signal shown in Fig. 2(d): $\tau_2=0$ fs (solid line), $\tau_2=200$ fs (dash-dot line), and $\tau_4=200$ fs (dashed line).

features seen along the $\tau_2=0$ fs axis in many tensor elements may reflect population dynamics. Of course, because we are speaking of low frequency intermolecular motions, the population dynamics we measure are likely a combination of the lifetimes for several of the excited states of these modes. While such population dynamics can appear on the $\tau_2=0$ fs axis, nonhyperpolarizability direct fifth-order signal cannot appear on the $\tau_4=0$ fs axis because the correlation function that governs it, $\langle [\alpha(\tau_2), \alpha(\tau_2)], \alpha(0) \rangle \rho$, will always be identically zero. So, in the absence of hyperpolarizabilities and residual cascade signals, the signal on the $\tau_2=0$ fs axis is a direct measure of population dynamics. While the $\tau_4=0$ fs axis should have no signal, slices along

the τ_2 dimension for small values of τ_4 should carry information about the pure dephasing rate of the $|0\rangle\langle 1|$ coherence (as well as other low oscillator state coherences). Along both of these axes, however, hyperpolarizabilities may contribute, though choosing tensor elements wisely may diminish the size of these hyperpolarizability signals. When this is the case, the interesting direct fifth-order signals near and on the $\tau_2=0$ fs axis and near the $\tau_4=0$ fs axis may be examined directly.

Feynman diagrams, such as those shown in Figs. 9(d) and 9(e), show that away from the two time axes, and thus in an area not contaminated by hyperpolarizabilities, population-type dynamics may also be in evidence. Here, as the first time period increases, vibrational dephasing occurs, and the population-type signal along τ_4 will be diminished. Figure 1 of Ref. 50 shows a simulation, based on a harmonic system coupled to a bath, that displays these characteristics. The population-type signals generated solely through nonlinear polarizability that contribute to the measured signal off the axes are all generated via pathways with a zero quantum interaction occurring in the final step. Thus by using MFK-type analysis, the tensor elements that weight pathways having the $\alpha^{(2)}$ interaction last most heavily should be those tensor elements that reflect population dynamics most strongly, just as the R_{zzmmzz} signal weights echolike diagrams most heavily. Of course, as seen in Fig. 9(e), anharmonicity-type diagrams can also give rise to population-type diagrams, and these cannot be analyzed through reference to the MFK PWDOSs.

One tensor element that appears to deselect for population-type dynamics is R_{yyzzzz} . In terms of hyperpolarizability signals, on the $\tau_2=0$ fs axis we expect to have a $\langle [\alpha_{yy}(\tau_4), \gamma_{zzzz}(0)] \rho \rangle$ interaction, and on the $\tau_4=0$ fs axis we expect to have a $\langle [\gamma_{yyzz}(\tau_2), \alpha_{zz}(0)] \rho \rangle$ interaction. The cascade simulation of this surface does have some contribution along the τ_2 and τ_4 axes, so if cascade residual terms are present, these residual cascade signals likely contaminate these areas. However, we assume cascade contributions everywhere are small, in part because the time dependence of the simulated cascades versus the measured signal on the axes indicates that cascade terms do not contribute significantly to the measured signal [Fig. 11(a)]. The cascade simulation of this surface, unlike the others presented, includes the contribution around time zero from the pure cascade terms that contribute to the back quadrant of the signal (where pulses three and four precede pulses one and two). The contribution in the back quadrant is different from that in the front quadrant, unlike in Ref. 25, because the phase matching geometry used here is not symmetric and because for this tensor element different third-order signals contribute to the cascades in the front and back quadrants. The back quadrant cascade signal has been explicitly included in this simulation because we present the $\tau_2=0$ fs slice, which clearly is affected by signal from the back quadrant. In addition to the apparent lack of cascades in our measured signal based on comparison to simulated cascades, our measured R_{yyzzzz} signal is qualitatively similar to that collected by Miller and co-workers in the first reported true heterodyne measurement of a direct fifth-order signal.²⁸ That experiment

was performed with a combination of 400 and 800 nm passively phase-locked pulse pairs produced with diffractive optics. The tensor element collected in that experiment, in which the signal was phase-selected for the direct fifth-order signal and thus phase-deselected for the cascades, was one in which the polarizations were all parallel for the excitation pulses and at 45° for the probe beam. The analyzer was set at 90° relative to the probe. In terms of our collected tensor elements this corresponds to a linear combination of the R_{yyzzzz} signal being discussed here and the R_{zzzzzz} tensor element discussed previously. Both our measured signal and their measured signal extend along the $\tau_2=0$ fs axis and are not pulse-width limited around that axis.²⁸

Our signal on the $\tau_4=0$ fs axis decays on the same time scale, approximately 120 fs when the square root of the data is fit to a single exponential, as the signal at $\tau_4=200$ fs [Fig. 11(b)]. Interestingly, the nonpulse-width limited signal around the $\tau_2=0$ fs axis decays on a similar time scale as well [Fig. 11(a)]. This slice has been fit to an exponential with a time constant of 200 fs, although data were not taken to long enough times in any of these slices to accurately fit the long time decay. Instead, such time constants are useful in relative terms to compare the time scale of decay of various slices fit over the same time range. The similarity between the decay times of the signals on the τ_2 and τ_4 axes suggests that these signals are governed by the hyperpolarizabilities as opposed to being governed by a hyperpolarizability along the $\tau_4=0$ fs axis and a $\langle[\alpha(\tau_4),\alpha(0)],\alpha(0)]\rangle$ type interaction along the $\tau_2=0$ fs axis. These two signals would presumably have different decay times because of the different weightings of the dynamics by the two types of signals, although as will be discussed below, such a distinction is less obvious for intermolecular modes than for high frequency vibrations. The fact that hyperpolarizabilities may govern the signal on both axes in this tensor element may be less surprising than in other tensor elements since here we expect the signal generated through the three-point polarizability correlation function to be quite small based on the PWDOS calculations. A weak three-point polarizability governed direct fifth-order signal on the $\tau_2=0$ fs axis would not preclude relatively strong hyperpolarizability signals on the axes. The very fast time constant associated with decay on the time axes is somewhat unexpected from a hyperpolarizability signal, though, since it resembles a third-order $\langle[\alpha^{(1)},\alpha^{(1)}]\rho\rangle$ type interaction. Heterodyne third-order measurements of CS_2 , dominated by $\langle[\alpha^{(1)},\alpha^{(1)}]\rho\rangle$ interactions, can be fit to an exponential with a time constant of 1.6 ps for times beyond 2 ps.⁴² However, the third-order signal's apparent time scale drops appreciably (to time scales of ~ 300 fs) when fit to the same time scale range (250–600 fs) over which we fit the slices from our two-dimensional signal. Also, the decay along the $\tau_2=0$ fs axis of this tensor element is significantly faster than the decay of that axis's signal in other tensor elements measured. This indicates that the other tensor elements have a different proportion of contributions on that axis from the direct population-type fifth-order signals compared to the hyperpolarizabilities, with the population-type signals more important in those tensor elements. If we are indeed seeing the hyperpolarizabilities on

the axes of the R_{yyzzzz} signal, the fast time scale decay seen in each of these slices relates to the vibrational pure dephasing time scale of liquid CS_2 and shows that the hyperpolarizability signals may probe the same dynamics as third-order measurements.

The tensor element collected that appears to weight for population dynamics is the $R_{yzzzzzy}$ signal shown in Fig. 2(d). This signal looks remarkably similar to the R_{yzzzyz} signal collected by Tokmakoff and co-workers in a passively phase-locked intrinsically heterodyne measurement of the direct fifth-order signal.²⁷ This signal should be identical to our $R_{yzzzzzy}$ signal by Kleinman symmetry.^{35,36} Aside from a small difference in peak position along τ_4 , the two measurements (when taking the square root of our data so as to compare the amplitudes of the signals) look virtually identical. Figure 12(b) shows slices from our collected surface. The square roots of the slices along τ_4 have also been fit to single exponentials. Here the signals were collected to longer times than in the R_{yyzzzz} signal, although still not long enough to accurately fit the long time decays. The $\tau_2=0$ fs and the $\tau_2=200$ fs slices were fit with time constants of approximately 2 ps and 1.6 ps, respectively, when fitting over the time range of 1000–1500 fs. When third-order heterodyne CS_2 data are fit over the same time range, it is best fit to an exponential with a time constant of approximately 1.2 ps. So, the data in this region of the $R_{yzzzzzy}$ signal appear to be decaying more slowly than third-order CS_2 data that at long times probes the molecular reorientational dynamics of the liquid. On the other hand, the signal at $\tau_4=200$ fs decays very quickly, much like that of the R_{yyzzzz} signal, potentially probing the same dynamics as seen in all discussed slices of that tensor element. Then, the presence of the slowly decaying features in the signal may be an indication that what is selected for in this tensor element is a population-type pathway of the direct fifth-order signal. A perusal of all the other signals presented, excepting the R_{yyzzzz} signal discussed above, strongly suggests that the long lived signals along the $\tau_2=0$ fs axes are indeed probing population dynamics, and this signal is dominated by $\langle[\alpha(\tau_4),\alpha(0)],\alpha(0)]\rho\rangle$ type interactions.

When examining the signal on the $\tau_2=0$ fs axis of the $R_{yzzzzzy}$ tensor element, we must of course consider both potential hyperpolarizability and cascade contributions along that axis. In the case of the $R_{yzzzzzy}$ signal, the expected hyperpolarizability signal is $\langle[\alpha_{yz}(\tau_4),\gamma_{zzzy}(0)]\rho\rangle$ on the $\tau_2=0$ fs axis. It previously had been suggested that such a hyperpolarizability signal (in which the γ interaction has an odd number of y and z indices) would be zero.¹⁰ While the rotationally averaged γ_{zzzy} would be zero, the signal we measure does not include a rotational average of γ_{zzzy} alone. So, we cannot maintain that hyperpolarizability signals should not be present in the $R_{yzzzzzy}$ tensor element based on symmetry arguments. Further, as in the case of the R_{yyzzzz} signal, we assume cascades everywhere are small, and this is supported by the full cascade simulation of this tensor element, which does not resemble the measured signal in either shape or time scale of decay [Fig. 12(a)]. So, while the hyperpolarizability signal likely contributes to a certain extent, the remarkable consistency between all the tensor elements

(except R_{yyzzzz}) in their extension along the $\tau_2=0$ fs axis strongly suggests that we are truly seeing population dynamics as probed by direct fifth-order processes along that dimension.

Further, neither the hyperpolarizability signal nor the presence of cascades can explain the most striking feature of the measured R_{yzzzzy} signal, the off-axis extension along τ_4 . This feature of the signal looks very much like the simulation of Fig. 1 of Ref. 50 and suggests that this tensor element may be weighting population dynamics heavily. Another possibility has been suggested by Golonzka *et al.* to explain the presence of this feature in their signal. They suggest that the long time signal present is related to molecular reorientations or cross-correlations between molecular reorientations and interaction-induced effects.²⁷ While it is certainly possible that some tensor elements would weight these dynamics more heavily than others, it is completely unclear at this point why these dynamics would only appear along the τ_4 time period of a tensor element that probed said dynamics. On the other hand, attributing this feature of the R_{yzzzzy} signal to population dynamics is more attractive because one can easily understand why this feature should be present for long times along the τ_4 dimension for small values of τ_2 [Fig. 9(c)]. Additionally, the fifth-order signal is expected to weight higher frequency motions more heavily than is the third-order signal, and thus we would be less likely to see long-time reorientations in the fifth-order signal than in third-order measurements.^{21,22}

Of course, in the case of the low frequency intermolecular motions of CS₂ that we probe, it is not obvious that population relaxation time scales and pure dephasing time scales should follow the trend seen in high frequency vibrations. In the case of high frequency vibrations, the large mismatch in frequencies between the interrogated oscillator and the bath modes causes population relaxation to be significantly slower than pure dephasing. The processes of population relaxation and pure dephasing are often thought of in terms of inelastic and elastic collisions, respectively: population relaxation comes about due to inelastic collisions in which there is energy exchange with the bath, and pure dephasing comes about due to elastic collisions in which only the phase of the wavefunction of the oscillator of interest changes.⁵⁰ For high frequency vibrations it is the energy mismatch between the vibration and the solvent bath modes that results in the inelastic processes being much less efficient than the elastic ones that result in rapid pure dephasing. The intermolecular motions of CS₂, on the other hand, function in this model as both the chromophore and the bath, and there is a continuous spectral density. However, despite the fact that the mismatch in frequencies between the oscillator of interest and the bath no longer exists, it does still appear that this separation of time scales holds for this system. This is seen in the time scales of the decay of the direct fifth-order signal from the intermolecular motions of CS₂ along the $\tau_2=0$ fs axis, where the three-point polarizability correlation function can only give rise to population-type Liouville pathways. The signals on this $\tau_2=0$ fs axis are significantly longer lived than any other portions of the signal, all of which must include dephasing effects before any population is created. (These

observations hold true for all but the R_{yyzzzz} signal.)

Attributing the extended features of the R_{yzzzzy} signal to population dynamics also allows us to turn to the MFK PWDOs to attempt to explain why a particular tensor element would weight such dynamics heavily. In terms of the MFK PWDOs, to heavily weight population dynamics pathways, either the $\alpha^{(2)}$ interaction would occur last or that tensor element would be dominated by anharmonically generated signal. According to the PWDOs generated by MFK, the tensor element most likely to weight the types of diagrams with the $\alpha^{(2)}$ interaction last is R_{mmzzzz} . The fact that we see no indication of population-type dynamics in that signal suggests the R_{yzzzzy} signal may be generated mostly through anharmonicity, though there is no obvious reason why this should be more true of this tensor element than of others. One assumption MFK make that could contribute to the differences between experiment and theory seen here is that signals due to the $\alpha^{(2)}\alpha^{(2)}\alpha^{(2)}$ interactions are not included. Such a signal could be described by the Feynman diagram shown in Fig. 9(f), and this clearly could give rise to population dynamics along τ_4 . If this contribution were significant for the R_{yzzzzy} tensor element, this could explain the observed signal. If indeed the signal in this tensor element is weighting population dynamics more heavily than dynamics described by other Feynman diagrams, it is clear that more attention in tensor analysis should be given to the possibilities for signal generation and weighting that have not yet been studied in depth: these include the $\alpha^{(2)}\alpha^{(2)}\alpha^{(2)}$ type interactions and anharmonically generated signal. Another interesting aspect of the extended feature of this tensor element that can not currently be explained either by understanding this feature as molecular reorientation/interaction-induced cross-terms or as population dynamics is that the peak of the feature as a function of τ_2 moves to progressively lower τ_2 values as τ_4 increases. This ‘‘lean’’ in the response implies a progressive decrease in the amplitude of lower frequency components in the response as τ_4 increases. Thus an understanding of this feature could give detailed insight into the frequency dependence of the liquid’s relaxation processes.

V. CONCLUDING REMARKS

The various tensor elements collected in the geometry designed expressly to suppress all cascade contributions to the measured fifth-order signal indeed appear to be dominated by direct fifth-order signal. This appears to be true even of the R_{zyzyzz} signal, which is expected to be the smallest according to the calculations of MFK. It does appear that in some tensor elements collected there is still a small amount of contamination by cascade signals. This contamination is now believed to arise predominantly from pure cascade terms and not from cascade/direct fifth-order cross-terms. These contributions could be diminished even further in a perfectly executed heterodyne detected measurement performed in a geometry such that all of the cascades and the direct fifth-order signal were perfectly phase matched. Then, the direct fifth-order signal field would be 90° out of phase with the cascade signal field and could be selected for with phase-sensitive detection. However, the probe pulse must be

phase-locked in relation to the local oscillator for this to be accomplished. This is difficult experimentally and has been approached through the use of diffractive optics elsewhere.^{27,28} We are currently pursuing this through the use of an actively phase-locked interferometer.⁵¹ In addition, using phase-sensitive detection with such a geometry in order to eliminate cascade contamination is complicated by the fact that the portion of the signal due to anharmonicity is expected to be delayed along the second time period with respect to the portion of the signal due to non-linear polarizability. It is further complicated by the potential dichroic response present in the third-order responses (comprising the cascade signals) that could alter the phase of the cascade signals from the expected 90° with respect to the direct fifth-order signal. The ideal experiment would use a geometry (such as the one used in these experiments) that quite effectively eliminates the cascades and *then* would use phase-selected heterodyne detection to ensure selection of the direct fifth-order signal alone.

Such a geometry and detection scheme would also allow for potential separation of the contributions to the direct fifth-order signal from anharmonicity and nonlinear polarizability. This is because the anharmonic signals must be delayed in the second time period with respect to the signals generated through nonlinear polarizability. Such time delays would be very short and potentially the two types of signals would be separable for signals collected with the same τ_2 period, varying τ_4 and phase-selecting for signal at each point after that. Of course, this potential separation would be of utmost interest and would also allow us to confirm or deny the importance of one of the variables that must be dealt with in comparing our data to the MFK simulations, which only include signal generated through nonlinear polarizability. Distinctions between our experimental observations and their predicted results may be explainable if we can measure the two parts of the signal separately and/or confirm that the anharmonically generated signal is very small. If this is the case, then the discrepancies between experiment and theory can be looked at in more detail: this may come through using INM simulations to fully consider such contributions currently considered to be small, such as the $\alpha^{(2)}\alpha^{(2)}\alpha^{(2)}$ interactions or signal due to $\alpha^{(2)}$ interactions that come from the first pulse pair. It may also be necessary to look in more detail at the full MD simulations that do not have the limitations that INM simulations have when considering longer time motions. This may be especially true for considering tensor elements such as R_{zzmmzz} . This tensor element extends to relatively long times in comparison to the inverse frequency of the probed modes and shows echolike character that allows us to put a limit of ~ 400 fs on the rephasing time scale of room temperature liquid CS₂. Further, the R_{yzzzyy} signal, which may highlight population dynamics, also extends to long times: analysis beyond INM simulations could confirm whether this tensor element selectively weights for population dynamics or if molecular reorientation/interaction-induced correlations are responsible for the extension along the τ_4 dimension. Such theoretical information will help us determine how well various slices of our direct fifth-order signal can separate pure dephasing from popula-

tion dynamics, one of the most interesting applications of this experiment.

ACKNOWLEDGMENTS

This research was supported by a grant from NSF. The authors wish to thank Professor J. Fourkas and Professor R. A. Harris for helpful discussions. We also acknowledge Professor R. Stratt, Professor R. J. D. Miller, and Professor A. Tokmakoff for useful discussions and for providing preprints of their papers.

- ¹ Y. Tanimura and S. Mukamel, *J. Chem. Phys.* **99**, 9496 (1993).
- ² S. Mukamel, A. Piryatinski, and V. Chernyak, *J. Chem. Phys.* **110**, 1711 (1999).
- ³ V. Chernyak and S. Mukamel, *J. Chem. Phys.* **108**, 5812 (1998).
- ⁴ K. Tominaga, G. P. Keogh, Y. Naitoh, and K. Yoshihara, *J. Raman Spectrosc.* **26**, 495 (1995).
- ⁵ K. Tominaga and K. Yoshihara, *Phys. Rev. Lett.* **74**, 3061 (1995).
- ⁶ K. Tominaga and K. Yoshihara, *J. Chem. Phys.* **104**, 4419 (1996).
- ⁷ K. Tominaga and K. Yoshihara, *J. Chem. Phys.* **104**, 1159 (1996).
- ⁸ A. Tokmakoff, M. J. Lang, D. S. Larsen, G. R. Fleming, V. Chernyak, and S. Mukamel, *Phys. Rev. Lett.* **79**, 2702 (1997).
- ⁹ A. Tokmakoff, M. J. Lang, D. S. Larsen, and G. R. Fleming, *Chem. Phys. Lett.* **272**, 48 (1997).
- ¹⁰ A. Tokmakoff and G. R. Fleming, *J. Chem. Phys.* **106**, 2569 (1997).
- ¹¹ A. Tokmakoff, M. J. Lang, X. J. Jordanides, and G. R. Fleming, *Chem. Phys.* **233**, 231 (1998).
- ¹² T. Steffen, J. T. Fourkas, and K. Duppen, *J. Chem. Phys.* **105**, 7364 (1996).
- ¹³ T. Steffen and K. Duppen, *J. Chem. Phys.* **106**, 3854 (1997).
- ¹⁴ T. Steffen and K. Duppen, *Phys. Rev. Lett.* **76**, 1224 (1996).
- ¹⁵ T. Steffen and K. Duppen, *Chem. Phys. Lett.* **273**, 47 (1997).
- ¹⁶ T. Steffen and K. Duppen, *Chem. Phys. Lett.* **290**, 229 (1998).
- ¹⁷ T. Steffen and K. Duppen, *Chem. Phys.* **233**, 267 (1998).
- ¹⁸ S. Saito and I. Ohmine, *J. Chem. Phys.* **108**, 240 (1998).
- ¹⁹ K. Okumura and Y. Tanimura, *J. Chem. Phys.* **107**, 2267 (1997).
- ²⁰ R. L. Murry and J. T. Fourkas, *J. Chem. Phys.* **107**, 9726 (1997).
- ²¹ R. L. Murry, J. T. Fourkas, and T. Keyes, *J. Chem. Phys.* **109**, 7913 (1998).
- ²² R. L. Murry, J. T. Fourkas, and T. Keyes, *J. Chem. Phys.* **109**, 2814 (1998).
- ²³ S. Mukamel, A. Piryatinski, and V. Chernyak, *Acc. Chem. Res.* **32**, 145 (1999).
- ²⁴ M. Cho, D. A. Blank, J. Sung, K. Park, S. Hahn, and G. R. Fleming, *J. Chem. Phys.* **112**, 2082 (2000).
- ²⁵ D. Blank, L. Kaufman, and G. R. Fleming, *J. Chem. Phys.* **111**, 3105 (1999).
- ²⁶ D. J. Ulness, J. C. Kirkwood, and A. C. Albrecht, *J. Chem. Phys.* **108**, 3897 (1998).
- ²⁷ O. Golonzka, N. Demirdoven, M. Khalil, and A. Tokmakoff, *J. Chem. Phys.* **113**, 9893 (2000).
- ²⁸ V. Astinov, K. J. Kubarych, C. J. Milne, and R. J. D. Miller, *Chem. Phys. Lett.* **327**, 334 (2000).
- ²⁹ D. A. Blank, L. J. Kaufman, and G. R. Fleming, *J. Chem. Phys.* **113**, 771 (2000).
- ³⁰ K. Okumura and Y. Tanimura, *J. Chem. Phys.* **106**, 1687 (1997).
- ³¹ M. T. Asaki, C. Huang, D. Garvey, J. Zhou, H. Kapteyn, and M. Murnane, *Opt. Lett.* **18**, 977 (1993).
- ³² T. Joo, Y. W. Jia, and G. R. Fleming, *Opt. Lett.* **20**, 389 (1995).
- ³³ J. C. Kirkwood, D. J. Ulness, A. C. Albrecht, and M. J. Stimson, *Chem. Phys. Lett.* **293**, 417 (1998).
- ³⁴ S. Mukamel, *Principles of Nonlinear Optical Spectroscopy*, 1st ed. (Oxford University Press, New York, 1995).
- ³⁵ R. W. Hellwarth, *Prog. Quantum Electronics* **5**, 1 (1977).
- ³⁶ M. Levenson and S. Kano, *Introduction to Nonlinear Laser Spectroscopy; Revised Edition* (Academic, San Diego, 1988).
- ³⁷ A. Tokmakoff, *J. Chem. Phys.* **105**, 1 (1996).
- ³⁸ A. Tokmakoff, *J. Chem. Phys.* **105**, 13 (1996).
- ³⁹ M. Cho, in *Advances in Multi-Photon Processes and Spectroscopy*, Vol.

- 12, 1st ed., edited by S. H. Lin, A. A. Villaeys, and Y. Fujimura (World Scientific, Singapore, 1999).
- ⁴⁰J. Sung and M. Cho, *J. Chem. Phys.* **113**, 7072 (2000).
- ⁴¹W. T. Lotshaw, D. McMorrow, N. Thantu, J. S. Melinger, and R. Kitchenham, *J. Raman Spectrosc.* **26**, 571 (1995).
- ⁴²D. McMorrow, N. Thantu, J. S. Melinger, S. K. Kim, and W. T. Lotshaw, *J. Phys. Chem.* **100**, 10389 (1996).
- ⁴³S. Ruhman, A. G. Joly, and K. A. Nelson, *IEEE J. Quantum Electron.* **24**, 460 (1988).
- ⁴⁴J. Etchepare, G. A. Kenney-Wallace, G. Grillon, A. Migus, and J. P. Cahmbaret, *IEEE J. Quantum Electron.* **QE-18**, 1826 (1982).
- ⁴⁵J. Etchepare, G. Grillon, and J. Arabat, *Appl. Phys. B: Photophys. Laser Chem.* **49**, 425 (1989).
- ⁴⁶B. Dick, *Chem. Phys.* **113**, 131 (1987).
- ⁴⁷T. I. C. Jansen, J. G. Snijders, and K. Duppen, *J. Chem. Phys.* **113**, 307 (2000).
- ⁴⁸A. Ma and R. Strat, *Phys. Rev. Lett.* **85**, 1004 (2000).
- ⁴⁹I. D. Hands, S. Lin, S. R. Meech, and D. L. Andrews, *J. Chem. Phys.* **109**, 10580 (1998).
- ⁵⁰D. W. Oxtoby, *J. Chem. Phys.* **70**, 2605 (1979).
- ⁵¹S. Matsuo and T. Tahara, *Chem. Phys. Lett.* **264**, 636 (1997).